Vera Rita Costa Salgado

Licenciatura em Ciências da Engenharia Biomédica

Analysis of functional Magnetic Resonance data for neurosurgical planning: subject specific resting state analysis as a complement to task based analysis.

Dissertação para obtenção do Grau de Mestre em

Engenharia Biomédica

Orientador: Alexandre Andrade, Doutor,
Instituto de Biofísica e Engenharia Biomédica, Faculdade de Ciências da Universidade de Lisboa

Júri

Presidente:	Doutora Carla Maria Quintão Pereira
Arguente:	Doutor Ricardo Nuno Pereira Verga e Afonso Vigário
Vogal:	Doutor Alexandre da Rocha Freire de Andrade

FACULDADE DE CIÊNCIAS E TECNOLOGIA
UNIVERSIDADE NOVA DE LISBOA

September, 2016

Analysis of functional Magnetic Resonance data for neurosurgical planning: subject specific resting state analysis as a complement to task based analysis.

Este documento foi gerado utilizando o processador (pdf)LaTeX, com base no template "unlthesis" [1] desenvolvido no Dep. Informática da FCT-NOVA [2]. [1] https://github.com/joaomlourenco/unlthesis [2] http://www.di.fct.unl.pt

Aos meus pais, irmão e avó.

Acknowledgements

First of all, I would like to thank the Institute of Biophysics and Biomedical Engineering (IBEB), where this dissertation was conducted, for all the support provided during this time.

I want to express my deepest gratitude to my supervisor, Alexandre Andrade. His guidance, support and availability were crucial for the success of this project. I am sincerely thankful for all the knowledge and experience achieved working with him.

I would also like to thank Dr. Martin Lauterbach, for the attentiveness and valuable contribution to this study.

To my parents, Cristina and José, I would like to say how grateful I am for all the emotional support and encouragement, not only in the last few months, but during my whole life. Thank you for the values that you transmitted, they are now far more treasured than ever. With the same gratitude I also would like to mention my brother, Francisco, for being supportive in his funny, but lovely way, and to my grandmother for all the knowledge and for being a role model my entire life.

To all people whom I shared my workspace with, I am thankful for all the assistance, dedication and companionship. Without you my lunch time would be certainly shorter but I wouldn't have so many memorable moments to share. I thank each and every one of you for helping me in different occasions, giving me the support I needed and for making this experience a remarkable one.

I also should not forget those who joined me in my academic journey. Your companionship will not be forgotten.

Finally, I would like to thank my hometown friends, the ones that I grew up with. Thank you for understanding my absence during the last 5 years. I know you are, as you always have been, rooting for my success.

The limited space of this acknowledgment section does not allow me to thank properly all the people who helped me achieve this new stage of my academic path. I will always cherish your friendship and think of you with fond memories. To all such people in my life, I am sincerely grateful.

Abstract

Brain and other central nervous system tumors are the 17th most common cancer type in Europe, being associated with high mortality rate. Neurosurgery has been the ultimate solution for the treatment of brain tumors. Integration of preoperative brain mapping in the process is highly recommended in order to preserve fundamental areas of the brain, especially those believed to be connected to language and movement. Recently, there has been a growing interest in presurgical planning resorting to resting-state functional magnetic resonance imaging (fMRI).

The aim of this thesis is to explore strategies to process data of resting-state fMRI in order to better understand its connection to task brain networks, and to assess their application to the protocols currently used within clinical institutions that are partners of the host scientific institution in an ongoing project. A total of 8 subjects were recruited to participate in this study, all of them previously referred for surgical tumor resection. An optimal strategy for pre-processing was devised and tested. Task data was processed using the General Linear Model, while rest data was processed through Independent Component Analysis. The processed data were then correlated via similarity coefficients.

The results of similarity tests show a limited coincidence between resting-state networks and the activation task areas. Further studies will be required in order to improve these results.

Keywords: Brain tumors, fMRI, General Linear Model, Independent Component Analysis, resting-state

Resumo

Os tumores cerebrais, juntamente com outros tumores do sistema nervoso central são o 17º tipo de cancro mais comum na Europa, estando associados a uma elevada taxa de mortalidade. A neurocirurgia tem sido uma das soluções para o seu tratamento. Neste âmbito, a integração do mapeamento cerebral pré-cirúrgico no processo é altamente recomendada a fim de preservar áreas fundamentais do cérebro, nomeadamente as que estão relacionadas com a linguagem e com o movimento. Recentemente, tem havido um crescente interesse no planeamento pré-cirúrgico com recurso à imagem de ressonância magnética funcional em repouso.

O objetivo desta tese é explorar estratégias para processar dados de ressonância magnética funcional em repouso, com o intuito de compreender a sua relação com redes cerebrais provenientes de paradigmas de tarefa, e explorar a aplicabilidade dessas estratégias nos protocolos actualemnte usados nas instituições clínicas associadas à instituição de acolheminto, no contexto de um projecto em curso. Um total de 8 indivíduos foram recrutados para participar neste estudo, todos eles previamente referenciados para resseção cirúrgica do tumor. Foi concebida e testada uma estratégia otimizada para o pré-processamento. Os dados de tarefa foram processados utilizando o Modelo Linear Geral, ao passo que os dados de repouso foram processados através da análise de componentes independentes. Os dados processados foram posteriormente correlacionados através de coeficientes de similaridade.

Os resultados dos testes de similaridade mostram uma coincidência limitada entre as redes de repouso e as áreas de ativação provenientes de paradigmas de tarefa. Serão necessários mais estudos de forma a melhorar estes resultados.

Palavras-chave: Análise em componentes independentes, Imagem por Ressonância Magnética Funcional, Modelo Linear Geral, Repouso, Tumores cerbrais.

Contents

List of Figures

List of Tables

Acronyms

BET brain extraction tool.

BOLD blood oxygenation level dependent.

CNS central nervous system.

CSF cerebrospinal fluid.

DICOM Digital Imaging and Communications in Medicine.

DMN default-mode network.

DNA deoxyribonucleic acid.

DPABI Data Processing and Analysis for Brain Imaging.

DPARSFA Data Processing Assistant for Resting-State fMRI- advanced edition.

DSC Dice similarity coefficient.

ECS electrical cortical stimulation.

EEG electroencephalography.

FD frame-wise displacements.

fMRI functional magnetic resonance imaging.

FWE familywise error.

FWHM full width at half maximum.

GIFT Group independent component analysis (ICA) of functional magnetic resonance imaging (fMRI) toolbox.

GLM General Linear Model.

hrf hemodynamic response function.

IC independent component.

ICA independent component analysis.

MEG magnetoencephalography.

MNI Monreal Neurological Institute.

MRI magnetic resonance imaging.

NIfTI Neuroimaging Informatics Technology Initiative.

PC principal components.

PCA principal component analysis.

PET positron emission tomography.

ReML restricted maximum likelihood.

REST Resting-State fMRI Data Analysis Toolkit.

Rf Radiofrequency.

rs-fMRI resting state functional magnetic resonance imaging.

RSN resting state networks.

SMN sensorimotor network.

SN salience network.

SPM Statistical Parametric Mapping.

TE echo time.

TR repetition time.

WM white matter.

Chapter 1

Introduction

Tumors of the central nervous system are associated with a high incidence and mortality rate. In 2012, brain and other central nervous system cancer was reported to be the 17th most common cancer type and the 12th most common cause of cancer death worldwide. Neurosurgery has been the ultimate solution for the treatment of these pathologies, with really satisfactory outcomes [1]. Nevertheless, in those circumstances, integration of preoperative brain mapping in the process is highly recommended in order to preserve fundamental areas of the brain, especially those believed to be connected to language and movement, denominated eloquent areas, and reduce post-operative deficits [2] [3]. In this scope, the search for an accurate knowledge about the structure and functionality of the brain has been one of the most important challenges for pre-planning neurosurgery.

In the early ages of neurosurgery only standard structural and functional maps were used to help neurosurgical planning. However, according to several scientific studies, the association between anatomical and functional areas shows high inter- subject variability [4]. Functional connectivity using fMRI, possibly complemented with other non-invasive imaging methods like electric source imaging (EEG), magnetoencephalography (MEG), positron emission tomography (PET), single photon emission computed tomography (SPECT) and functional magnetic resonance imaging (fMRI) has been adopted in order to trace network connections that are subject-specific and therefore to provide additional information that is useful for presurgical mapping [5] [2]. More specifically,

fMRI, as an innocuous approach, has proven to be a promising technique to acquire the activation sites of the human brain involved in the eloquent functions, through assessment of changings in blood oxygenation level dependence (BOLD) [3]. Typically, fMRI appraises small hemodynamic fluctuations induced by stimulus or by task performance [3] [6].

Nonetheless, recent developments led to the belief that there is a temporal and functional correlation among separated brain regions, responsible for behavioral and cognitive functions control, even in rest conditions. In addition, there are small changes in BOLD signal during rest that confirm an incessant interaction between brain networks, thus leading to Resting-State Network [2] [3] [7]. Despite the increasing interest in this new approach, there is still a long way ahead until resting-state fMRI is completely accepted and applied inside the clinical realm [8].

1.1 Objectives

The aim of this thesis is to explore strategies for resting-state fMRI data processing in order to better understand its relationship with brain networks from task paradigms and its contribution in improving diagnosis and pre-surgical planning. As a result, subjects unable to perform tasks, such as asleep or anesthetized patients, could benefit from this diagnostic technique, since it does not require the performance of any task. For this purpose, it is intended to test and optimize a preprocessing protocol, followed by the adaptation of some processing protocols used in the literature, devised for the task and rest data individually. Finally, it is intended to employ the results from these procedures in similarity analysis, aiming to realize the resemblance between brain activation in task performing and at rest, in order to test the reliability of resting state data analysis to complement the classic task approach in pre-surgical planning.

The work carried out within this thesis was hosted by the Institute of Biophysics and Biomedical Engineering of the Faculty of Sciences of the University of Lisbon, in the context of an ongoing collaboration with Sociedade Portuguesa de Ressonância Magnética/Hospital da Cruz Vermelha and Centro Hospitalar de Lisboa Norte/Hospital de Santa Maria.

1.2 Dissertation overview

This section aims to present a brief description of topics covered in each chapter in order to provide an enlightened reading.

Chapter 2. Background reviews the background literature related to the work developed in this dissertation. In particular, it provides some basic concepts about brain tumours, such as the brain mapping methodologies commonly used for surgical planning, which includes a description of functional magnetic resonance imaging ant its newest approach, resting state fMRI.

Chapter 3. Materials and methods details how the current study was conducted, undergoing a brief exposition of the software and methodology implemented. It also presents a brief description of the participants and the image acquisition protocol, followed by the detailed information about the methods and software used in the preprocessing and processing stages Finally, it is explained how the task based and resting state maps were superimposed such as its correlation calculation.

Chapter 4. Results intends to report the most relevant results obtained in preprocessing and processing stages, followed by the presentation of statistical and similarity analysis results.

Chapter 5. Discussion presents the analysis and discussion of the study results, as some limitations and suggestions for improvement.

Chapter 6. Conclusion provides the overall conclusions and suggestions for future work.

Chapter 2

Background

2.1 Brain Tumors - Basic Concepts

The human brain composes the central nervous system (CNS) along with the spinal cord and meninges. Taken together, they are responsible for controlling the majority of the bodily functions [9]. As with all other parts of the body, the CNS comprises numerous cells some of whose functions are managed by the deoxyribonucleic acid (DNA) , which is contained in their nuclei. When DNA carries a disability these functions may be compromised. More specifically, mutation of DNA can affect the production, growth and division cycle of cells, leading to an abnormal mass accumulation which compresses and damages the surrounding brain areas, commonly named as brain tumor or intracranial neoplasm [10].

Brain tumors are highly variable in shape, size and localization.They can be categorized as primary or metastatic. The first group refers to an abnormal mass that arises originally from the brain, whereas the second one refers to tumors that begin outside the CNS and then spread to the brain, such as metastasis from breast, lung and kidney cancer [11].

Brain tumors have their designations by the location in which they begin. Some of these are listed in table 2.1.

Treatment options vary with tumor location and severity. The most widely used alternatives are: **a)** radiation therapies, that use high energy beams of photons or particles

Table 2.1: Brain tumor classification [12] [13] [14]

<table>
<tr><th colspan="3">Brain Tumors Classification</th><th>Localization</th></tr>
<tr><td rowspan="6">Primary Brain Tumors</td><td rowspan="3">Gliomas</td><td>Astrocytomas</td><td>Glial cells - astrocytes.
Most often in the cerebrum</td></tr>
<tr><td>Oligodendrogliomas</td><td>Cells that make the fatty substance that covers and protects nerves.
It usually occurs in the cerebrum</td></tr>
<tr><td>Ependymomas</td><td>Cells that line the ventricles or the central canal of the spinal cord.</td></tr>
<tr><td colspan="2">Primary cerebral lymphoma</td><td>Lymphatic system</td></tr>
<tr><td colspan="2">Choroid plexus papillomas</td><td>Producer cells of cerebrospinal fluid, which are located in the ventricles.</td></tr>
<tr><td colspan="2">Haemangioblastomas</td><td>Posterior cranial fossa.</td></tr>
<tr><td colspan="3">Metastatic tumors</td><td>Another part of the body, such as lung, breast or kidney.</td></tr>
<tr><td colspan="3">Meningiomas</td><td>Meninges.</td></tr>
<tr><td colspan="3">Cranial nerve schwannomas</td><td>Supporting nerve cells called vestibular schwannomas</td></tr>
<tr><td colspan="3">Pituitary adenomas</td><td>Pituitary gland, that is located at the base of the brain.</td></tr>
</table>

to slow or stop the growth of the tumor; **b)** chemotherapy, that relies on the use of drugs to destroy cancer cells, usually by stopping the cancer cells' ability to grow and divide; and **c)** surgery, which includes complete or partial tumor resection [11] [15].

As a matter of fact, neurosurgery has been the ultimate solution for a number of subjects with brain tumors with really satisfactory outcomes[15]. Among other brain tumors, gliomas and metastases represent almost 60 % of brain tumor surgery, while meningiomas account for 20% and schwannomas and pituitary adenomas for 15% [12].

2.1.1 Eloquent Areas

Eloquent cortex refers to specific brain areas that directly control language, motor and sensory function. Therefore a precise assessment about function distribution over the

human brain is necessary for the presurgical planification. Damage to these areas generally leads to major neurological deficits. Brain areas responsible for motor function are mostly located in the precentral gyrus just anterior to the central sulcus. However, there are several other areas that are likewise relevant to body motion. Premotor and supplementary motor area include brain regions responsible for planning and controlling movement. Both of those areas are located in the mesial and lateral side of superior frontal gyrus, forward to precentral sulcus. The communication of those different areas throughout the corticospinal fiber tract is responsible for coordination and synchronicity of movements. [16].

Sensorial information follows the inverse pathway of motor function and it is mainly directed to the primary somatosensitive area, located in the postcentral gyrus, posterior to the central sulcus [17] [16].

Broca's area, believed to be one of the areas responsible for speech production, is anatomically located in the inferior frontal gyrus and it is composed by two areas: the pars triangularis and the pars opercularis. The function of Broca's area is to command the muscles so that they produce meaningful sounds. Broca's area is connected to Wernicke's area through a white-matter fiber tract called arcuate fasciculus. Wernicke's area is one of the areas responsible for language understanding. It's placed on the back portion of temporal lobe of the dominant hemisphere, that generally is the left hemisphere [17].

2.2 Surgical Planning

The challenge of brain lesions' surgical resection is balancing the aim of maximizing resection with the requirement to preserve functionally-relevant brain areas, especially those believed to be connected to language and movement, denominated eloquent areas[16]. In this scope, accurate localization of those areas is essential for presurgical planning, as it helps optimize resection and decrease postoperative deficits [18] [6] [3].

2.2.1 Brain Imaging Techniques

In the early ages of neurosurgery only standard structural and functional maps were used to help neurosurgical planning. Nevertheless, according to several scientific studies, anatomical and functional areas have high inter-subject variability owing, not only, to individual characteristics of cortical organization, but also to functional reorganization in response to the individual's brain pathology [4] [19]. This inconstancy among

subjects led to a growing concern to develop new imaging techniques capable of creating individual brain maps.

The first subject specific's functional mapping procedure was an extremely invasive technique, called Intracarotid Amobarbital procedure or Wada Test. During this intra-operative method, an anesthetic medication is injected into the right or left internal carotid artery putting that hemisphere to sleep and incapable to communicate with the opposite side [18]. The main goal of this procedure was to determine which side of the brain controls language function and how significant each hemisphere is in regard to memory function [20].

The Wada Test has been replaced or complemented by electrical cortical stimulation (ECS), another invasive procedure that resorts on stimulation of the cerebral cortex's surface while the patient is awake and performing motor, language or cognitive controlled tasks. This approach can only be used in intra-operatively stage and as it relies on the use of anesthetics it may produce unsatisfying outcomes [6] [20].

Regardless of whether the Wada Test or ECS are considered the gold standard procedures for mapping brain function, both require an awake and cooperative subject. Their invasive nature led to the need for non-invasive approaches. With the advent of high resolution non-invasive neuroimaging, there has been improved ability to map the structure of the brain, as well as its connections. In this scope, techniques such as fMRI, electroencephalography (EEG), magnetoencephalography (MEG) and positron emission tomography (PET) have been adopted in order to trace network connections that are subject-specific and therefore to provide profitable information for pre-surgical planning assessment [5] [2].

In a brief description, PET is based on the detection and imaging of positron-emitting radionuclides that were previously administrated to the patient. PET images demonstrate indirectly functional courses involved in cerebral metabolism. Like other techniques, such as computed tomography or magnetic resonance imaging (MRI), PET relies on reconstruction tecquniques to obtain tomographic images. In order to acquire better anatomic localization of the regions of interest PET images can be overlaid with anatomic images such as MRI or computed tomography [21].

As for the EEG, it is a direct measure of brain function which records the electrical activity of the brain resorting to electrodes that are placed on the subject's scalp. The time-series of scalp potential maps represent the differences in electric potential of distinct brain areas [2] [22].

Lastly, MEG measures the brain's neuronal activity recording its magnetic fields.

These magnetic fields are generated by neuronal electrical currents. The spatial distributions of the magnetic fields are analyzed in order to map brain regions involved in specific functions. Since the magnetic field measured by MEG is produced directly by electrical neuronal activity, it is possible to detect signals from the brain on a submillisecond time scale [23].

Although all brain mapping techniques should present identical outcomes, intermodal variations exist.

2.2.2 Magnetic Resonance Imaging

MRI is an imaging technique that relies on protons and their inherent magnetism to generate an image. As the human body is composed mainly of water, MRI takes advantage of the great abundance in hydrogen nucleus (^{1}H) by manipulating them with Radiofrequency (Rf) energy in the presence of a strong magnetic field [24].

The hydrogen atom consists of an orbiting electron and a single positively charged proton (nucleus) which spins around its axis, creating a magnetic moment along the direction of spins' axis. The sum of all the magnetic fields of each spin is called net magnetization. In the absence of an external magnetic field, the nuclei of hydrogen atoms in a sample are randomly distributed and therefore the sum of all the results in a null net magnetization. On the other hand, when exposed to a strong static magnetic field B_0, the nuclei will align parallel or anti-parallel to the field. As it requires less energy, the majority of the spins allign parallely with field B_0 creating a magnetization in that direction. The nuclei precess with an angular frequency determined by the Larmor frequency ω_0. The relation between Larmor frequency and the main magnetic field strength is displayed in the equation 2.1, where ψ represents the gyromagnetic ratio. Nevertheless, not all spins rotate in the same phase, therefore the sum of all the spins' transverse magnetizations is null.

$$\omega_0 = \psi \cdot B_0 \tag{2.1}$$

The phase equilibrium can be disturbed through a short oscilating magnetic field (i.e. radiofrequency pulse). Only protons that precess with the same frequency (Larmor frequency) as the electromagnetic Rf pulse will absorb energy, aligning their phases and thereby generating a component of the magnetization over the transversal plane (or xy plane). After the radiofrequency pulse is removed the system returns to equilibrium, in the process called dephasing, and there is recovery of the longitudinal component (z-direction) with an emission of electromagnetic energy.

Longitudinal relaxation corresponds to exponential recovery in longitudinal magnetization. It is characterized by the energy exchange between the spins and the surrounding environment. The recovery rate is a constant tissue-specific time generally called T1. On the other hand transversal relaxation is result of a progressive dephasing of nuclei following the RF pulse caused by a spin-spin interaction. This inter-dipole interaction time is an exponential decay in transversal magnetization and is designated by T2. The MRI ability to create anatomic images is due to the tissue-specific relaxation times, which enables the differentiation between different tissues.

In actual MRI procedures, the transversal relaxation time is shorter than T2. The inconsistency results from the inhomogeneities in the main magnetic field. This observed time, called T2*, has an essential role on functional Magnetic Resonance Imaging.

2.2.2.1 Functional Magnetic Resonance Imaging

In the last 25 years, the neuroimaging world had suffered several great updates and innovations. The discovery that MRI could be sensitive to brain activity, besides its anatomy, was probably the most remarkable one [25].

In regular brain imaging techniques the main goal is to distinguish different tissue types. Nonetheless, in functional brain imaging the purpose is to assess signal fluctuations over time. fMRI is one functional neuroimaging technique used to measure brain activity [26].

When a specific brain region increases its activity due to a task or a stimulation, the initial amount of oxygenated haemoglobin in the nearest blood vessels decreases, enhancing the deoxygenated haemoglobin. Seconds passed, there is a demanding need for additional oxygen and thus the blood flow increases, providing a great amount of oxygenated haemoglobin. fMRI is sensitive to this expansive rebound and the relative decrease in deoxyhemoglobin concentration, as it introduces a low increment in $T2^*$ weighted signal. This phenomenon is called blood oxygenation level dependent (BOLD).

The basic foundation of fMRI is the fundamental difference in the paramagnetic properties of deoxygenated and oxygenated haemoglobin. The hemoglobin molecule has magnetic properties that differ whether it is bound to oxygen or not. The oxygenated hemoglobin (Hb) has no unpaired electron and no magnetic moment (diamagnetic), therefore it is not magnetically distinct from other tissues. In contrast deoxyhemoglobin (dHb) has an unpaired electron and magnetic moment (paramagnetic) and thus deoxygenated blood differs in its magnetic properties from surrounding tissues [27].

fMRI has had a growing impact in neuroimaging. Since it is a non-invasive and an

ionizing radiation-free technique, fMRI can assess brain function safely. Besides, due to its good spatial resolution, fMRI has been broadly used in clinical settings. Alongside the pre-surgical planning, the use of this functional imaging method has played a key role in functional evaluation in brain tumor management [28], in the study of Parkinson's disease [29], as well as in early detection of Alzheimer's disease [30], and also in investigations of psychiatric disorders such as schizophrenia and severe depression [28]. More specifically, in pre-surgical context, fMRI demonstrates great precision in defining which hemisphere is language dominant, helping to decrease post-operative deficits, likewise reducing surgical time and improving the decision of the areas to recess.

Recent studies on spontaneous modulations in BOLD signal revealed the reproducibility of traditional fMRI in the absence of stimuli. These advances mean a new range of applications and prospects of fMRI and this topic will be explored in the next section.

2.2.3 Resting State functional Magnetic Resonance Imaging

The idea that human's brain is not idle in periods of resting has been explored since the IX century [31]. Nevertheless, it was only in the auspicious years for technological developments that followed the Second World War, when Seymour Kety and Carl Schmidt first measured whole-brain metabolism and blood flow [32]. Seymour and Schmidt realized that in rest conditions the brain consumes 20% of the body's energy, 10 times higher the expected value for only 2% of the body weight. Furthermore, in task performance, metabolic consumption only increases 5% [32]. This assumption makes clear the evidence of an intrinsic activity which expends the majority of the energy. Years later, the appearance of imaging techniques such as PET and fMRI brought new developments in the history of resting-state oscillations. Initially, slow spontaneous fluctuations in the BOLD-fMRI signal (typically < 0.1 Hz) were considered noise [33]. These artifacts, or so they thought, would be a result of non-neuronal sources like head motion [34]. Then, in 1995, Biswal and his colleagues were the first to demonstrate the functional implication of these fluctuations [35]. Biswal, trying to know what was the transfer function of the sensorimotor cortex, filtered out the respiration signal. The results showed that neither the respiration nor cardiac signal were the foremost contributors to the artifacts. In fact, they found that the main sources were lower-frequency signals. In an attempt to know what sources could provide a signal with that range of frequencies, they correlated a resting state time-series of a voxel from the sensorimotor cortex with the resting state time-series of every voxel in the brain. The results showed that the

strongest correlations were between the left and the right sensorimotor cortices [35]. Later studies confirmed the existence of synchronous fluctuations between other functional networks, like the primary visual network, auditory network and higher order cognitive networks [35] [36]. Biswal, in addition, showed that resting-state and task-based activation maps are notably similar [35]. These low frequency BOLD fluctuations observed while in resting show temporal correlations between anatomical distinct areas of the brain. These patterns have been designated "intrinsic connectivity networks" or "resting state networks".

Since initial contributions of Biswal up to the present day, the study of resting-state networks has shown a huge potential for the diagnosis of several pathologies like Alzheimer's, miultiple sclerosis, autism, Tourette syndrome among others [8].

Although the true origin of these resting state BOLD signal oscillations ($\sim 0.01 - 0.1Hz$) is not fully understood yet, it is proven that they are intrinsically generated by the grey matter and are not consequence of external stimulation.

2.2.3.1 Resting State Networks

The discovery of brain's resting state networks was accidental. Scans of resting-state brain started to be included in the task-paradigm studies as a baseline for comparison. However, investigators noticed that some brain regions were more active in resting conditions than in controlled task .

The first resting state network to be discovered was default-mode network (DMN). The default mode network, is a group of brain regions that shows higher levels of activity when the subject is not involved in any mental exercise. This network is responsible for memory consolidation, monitoring the environment, keeping awareness even when resting and other ongoing intrinsic thoughts. Anatomically, the regions involved on this network are generally the medial prefrontal cortex, posterior cingulate cortex, and the inferior parietal lobule. Other regions as the lateral temporal cortex, hippocampal formation, and the precuneus are also described in literature as being included in DMN [37]. For an enlightened interpretation consult figure 2.1.

Several other resting state networks (RSN) have been studied and described in literature. Although there is no concordance on names or localizations, there are 4 major resting-state networks in addition to DMN: auditory, visual, salience and sensorimotor network, see figure 2.2. Hereinafter are a brief description of them.

The auditory network has a major role on language comprehension and speech production, beyond acoustic processing such as tone distinctiveness and music. The

auditory network enfolds transverse temporal gyrus, also known by Heschl's gyrus, that contains the primary auditory cortex (Brodmann area 41), and also bilateral superior temporal gyri, and posterior insular cortex [38] [39].

Visual network can be decomposed in three sub-networks. The medial visual network is responsible for simple visual task, while lateral and occipital visual network is believed to be incorporated in high-order visual and emotional stimuli [38]. The visual network encompasses most of the occipital cortex [40].

The salience network (SN) consists of three main cortical areas: the dorsal anterior cingulate cortex, the left and anterior right insula (aRI), and the adjacent inferior frontal gyri. It is believed that SN is involved in coordination of behavioral responses, including switches between intrinsic attention (DMN) and task-related states, cognitive control and implementation of repeated tasks [38].

The sensorimotor network (SMN) is responsible for preparing the brain to perform a coordinated motor task. This specific network is anatomically divided into motor and sensory cortices. The primary motor cortex covers a region that starts in the bottom of the precentral sulcus and extendens to the bottom of the central sulcus, whereas the primary sensory area covers the bottom of the central sulcus up to the bottom of the postcentral sulcus [39], extending to the supplementary motor areas [38].

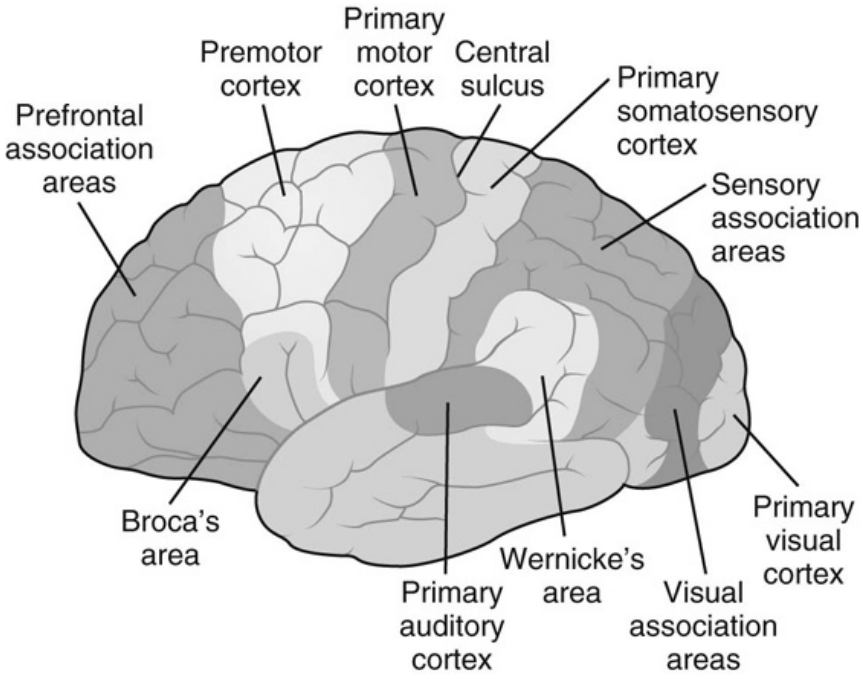

Figure 2.1: Classic anatomic sites for functional brain areas [41].

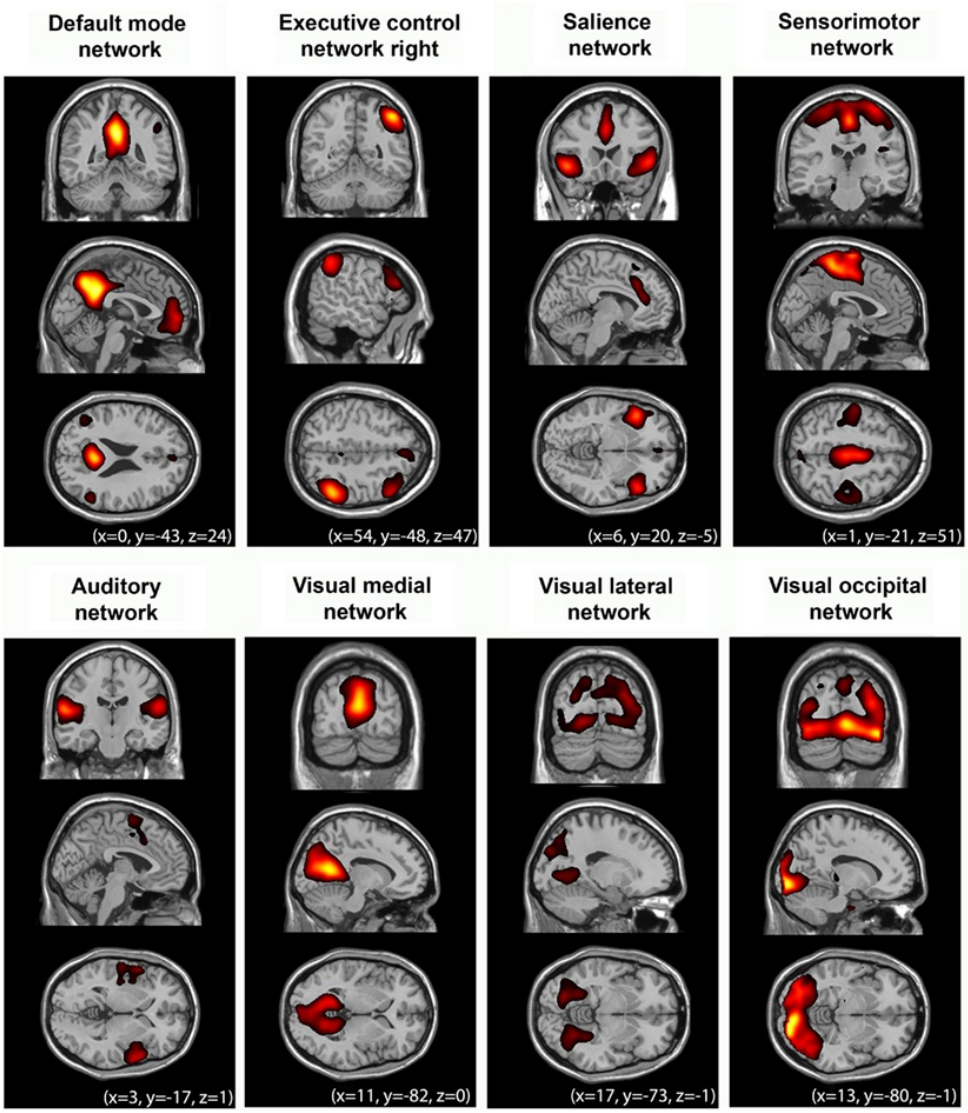

Figure 2.2: Resting-State networks [38]

2.2.4 fMRI processing

Recent studies have attempted to understand how the information contained in the rest maps can be applied in a clinical setting. A recurrent approach is the comparison between activation maps obtained at rest and activation task maps. The study of the correlation level between those is useful to understand how the resting-state fMRI can contribute to mapping major brain regions whose resection surgery should be minimized in order to ensure the subjects quality of life. Studies such as Sair et al. 2016,

Branco et al. (2016) and Tie et al. (2014) [42] [43] [44] focus on the study of language tasks maps and its similarity to rest maps. In all these studies, the methodology used for task image processing differs from resting images processing. In the first case, a classical approach to General Linear Model is used to extract the activated regions, whereas the second one is based on independent component analysis. Contextualization and information of these methods are described in the following sections.

2.2.4.1 Task: Statistical analysis and General Linear Model

General Linear Model (GLM) is a statistical linear model that aims to predict the variation of the dependent variables through a linear combination of several model functions plus error. The general linear model is a generalization of multiple linear regression model altough with more than one dependent variable.

In fMRI context, the dependent variables represent the time course of each voxel, Y, while the regressors, or predictors, that compose the design matrix correspond to time courses of what is believed to be fMRI responses towards tasks or head movements, equation 2.2. Each regressor X has an associated coefficient, β , which weights its contribution on the voxel time course Y. It is then necessary add an error value, ϵ, to offset noise fluctuation. That value is a random variable that is assumed to have a normal distribution of mean zero and variance value σ^2, equation 2.3. In every design matrix the first column, or the first regressor x_0, is constant and equals to 1. Its corresponding β_0 value is the signal at the starting conditions and it helps to model the main effect for the repeated measure factor on responses.

$$\begin{array}{ccccccccccc} y_1 = & \beta_0 x_0 & + & \beta_1 x_{11} & + & \cdots\cdots & + & \beta_p x_{1p} & + & \epsilon_1 \\ y_2 = & \beta_0 x_0 & + & \beta_1 x_{21} & + & \ldots\ldots & + & \beta_p x_{2p} & + & \epsilon_2 \\ \vdots & \vdots & & \vdots & & \vdots & & \vdots & & \vdots \\ y_n = & \beta_0 x_0 & + & \beta_1 x_{n1} & + & \cdots\cdots & + & \beta_p x_{np} & + & \epsilon_p \end{array} \tag{2.2}$$

$$\epsilon \sim N(0, \sigma^2) \tag{2.3}$$

The structural model for GLM is simply described by the following matrices notation

(equation 2.4) .

$$\begin{bmatrix} y_1 \\ y_2 \\ \vdots \\ y_n \end{bmatrix} = \begin{bmatrix} 1 & X_{11} & \cdots & \cdots & X_{1p} \\ 1 & X_{21} & \cdots & \cdots & X_{2p} \\ \vdots & \vdots & \cdots & \cdots & \vdots \\ 1 & X_{n1} & \cdots & \cdots & X_{np} \end{bmatrix} x \begin{bmatrix} \beta_0 \\ \beta_1 \\ . \\ \beta_p \end{bmatrix} + \begin{bmatrix} \epsilon_1 \\ \epsilon_2 \\ \vdots \\ \epsilon_n \end{bmatrix} \tag{2.4}$$

In order to assess if the hypothetical fMRI task responses correspond to real brain activations, GLM performs statistical data analysis.

Statistical data analysis allows to compute the difference among task activations and rest periods, comprising the amount of variability of the measured data points,i.e, the amount of noise fluctuations. Thus, assuming the null hypothesis, the probability of a randomly activation has occurred can be calculated.

A t-test is one of the statistical hypothesis tests that estimate the uncertainty of an activation. It describes the relationship between the mean of the observed difference of two effects (for example, activation and rest) with the variance of the noise fluctuations from the data, equation 2.5.

$$t = \frac{\overline{X_2} - \overline{X_1}}{\hat{\sigma}_{X_2 - X_1}} \tag{2.5}$$

For data with large noise fluctuations, the value of t is small, or in contrast, the higher the t value, the greater the likelihood that the observed mean difference is result of a true activation.

The p-value helps to determine the significance of the results. It represents the probability that the observed spatial pattern was created by some random process. Which means that if p is low, the observed mean difference exists, or in other words, it means that the activation occurred.

In neuroimaging, the number of statistical tests is massive, since each brain voxel constitutes a single test. Thus the significance of the results is questionable, since there is a high probability that there are false positives - multiple comparison problem. The balance between false positives and false negatives is accomplished by a p-value threshold. Neverthless, the standard p-threshold (0.05) may not produce the best outcome. For example, supposing a brain comprising 100000 voxels, it is expected that there are

5000 false positives. Therefore, it is common to correct the p-threshold - familywise error (FWE) correction. The FWE relies on the fundamentals of Bonferroni correction, but taking into consideration the spatial correlation between voxels, since the Bonferroni correction, which assumes statistical independence between the multiple tests would be too strict [45]. There are other correction approaches such as voxel-wise control of the false discovery rate and formal heuristics.

A different solution is apply a lower uncorrected threshold. A typical threshold is $p < 0.001$. This threshold may be too conservative and thus produce false negatives.

2.2.4.2 Resting-state fMRI data processing

Several techniques have been suggested to process resting state functional magnetic resonance imaging (rs-fMRI). Although these techniques have distinct methodological basis they can be distinguished into two major groups: model-dependent and model-free methods.

1. **Model-dependent method: seed method**
   Andrews-Hanna [46], Biswal [35], Cordes [36] and their respective colleagues studied functional connectivity applying seed-based methods. These techniques consist of correlating the resting-state time-series of a specific region of the brain against the times-series of all other brain's regions. The selected region is typically called seed and can be defined based on activation maps or anatomically, from an atlas. The result is a functional connectivity map defining the functional connections of the predefined seed. In spite of being a simple technique, the seed based approach only provides information of the functional connections of the selected region of interest [40] [47]. Instead of correlation, more sophisticated association measures can be used, such as coherence.

2. **Model-free methods**
   As opposed to the abovementioned approaches, model-free methods are able to assess functional connectivity of the whole brain. As these techniques don't require a predefined seed, they are conceived to search for patterns of connectivity across the brain. Among the numerous existing techniques, the most frequently mentioned in the literature are principal component analysis (PCA), ICA and normalized cut clustering.

Clustering strategies intend to gather variables with high level of similarity. Therefore, clustering outcomes may be more similar to traditional functional connectivity maps and consequently simpler to understand. Several clustering algorithms have been described. Hierarchical clustering, k-means and c-means algorithms are some of the most talked about in the literature [48] [49].

In contrast to the above mentioned method, PCA attempts to identify a reduced number of uncorrelated variables from a large set. These incoherent variables are usually designated as principal components (PC). The first PC reflects the linear combination of the components with highest variance and the following ones are the orthogonal components of the previous. PCA reveals the greatest amount of data's variance with the fewest number of PC [50]. PCA was used in studies headed by Friston [51] and Damoiseaux [52].

Lastly, ICA has been used in studies headed by Kiviniemi [53] and Beckmann [54]. The goal of this method is to search for sources of brain signal that are maximally independent from each other in order to separate spatial or temporally independent patterns from linearly mixed BOLD signals. One advantage of ICA has upon the seed approach is its aptitude of removing physiological and motion artifacts. The fundamentals of ICA are described in subsection 2.2.4.3.

2.2.4.3 Independent Component Analysis

fMRI datasets are composed by combinations of several physiological and external signals produced by different sources. Extracting the signals of interest is a big challenge once the signals are not static and could vary in space and over time. Independent Component Analysis (ICA) is one statistical technique for decomposing a complex dataset into subcomponents. It was first described by Comon in 1994 and it has been applied in many different fields. To better understand the theoretical design of this method it is common to resort to a cocktail party analogy. In a cocktail party, microphones are placed indistinctly over the room. Each microphone records a different signal, that results from the distance from each source, which in this example are the conversations and the music band playing. What ICA proposes to do is to decompose the signal recorded by each microphone into its different sources. Similarly, ICA has the same goal in Neuroimaging setting. But in this context, there is a time course of activity for each voxel. The goal of ICA is to decompose the spatial-temporal map into spatial and temporal components.

Mathematically, one can describe ICA using the following vector-matrix notation (equation 2.6).

$$x = A \cdot s \tag{2.6}$$

Where x contains the observed (mixed) signals, s is a two-dimensional random vector containing the independent source signals and A is the two-by-two mixing matrix. This algorithm can be described as a statistical "latent variables" model because the independent components and the mixing matrix cannot be directly observed, unlike x. Then ICA tries to find a linear transformation at the feature space x into a new feature space s, where each of the individual new features are mutually statistical independent and the mutual information from the new space and the original one is high as possible. In other words, x can be transformed into volume maps, s, by making linear combinations, defined by matrix W, of the volumes recorded at each time point.

$$s = W \cdot x \tag{2.7}$$

ICA orders its independent components by the most variance as the first one and continuing in descending order. This algorithm can be used in resting-state dataset, where different networks that seem to be correlated together can be identified, and also in a task-based approach, where high variance means a considerable amount of activity.

Chapter 3

Materials and methods

This chapter is intended to explain how the current study was conducted, undergoing a brief exposition of the software and methodology implemented. The chapter begins with a description of the subjects who participated in the study as well as the parameters of image acquisition. Then, detailed information about the methods and software used in the pre-processing of the acquired data is reported, followed by the explanation of the strategies used to process the images and to extract the activation networks of task and rest paradigms. Finally, it is explained how the neural maps were superimposed and its correlation calculation.

3.1 Participants and Image acquisition

This research gathered data provided by Hospital Cruz Vermelha. A total of 8 participants were recruited to participate in this study. All of them were previously referred for surgical resection of a brain lesion. The demographic characteristics of the participants are reported in table 3.1.

All patients were scanned using a 3-T (Philips Achieva by Philips Medical System, Netherlands). A gradient echo sequence was applied and the first three volumes were discarded in order to achieve a homogeneous magnetization. The data acquisition protocol consists of the following steps.

Structural images were obtained with a matrix of 256x256, 160 contiguous slices, voxel size of 1.8x1.8x4, flip angle = 8°, repetition time (TR)=11ms and echo time

Table 3.1: Demographic features of the study population

Subject ID	Sex	Age
Sub001	M	19
Sub002	M	26
Sub003	M	37
Sub004	M	33
Sub005	M	14
Sub006	M	31
Sub007	M	32
Sub008	F	35

(TE)=4.6ms.

Functional images were acquired with a matrix of 128x128 and a flip angle of 90°.

For the rs-fMRI acquisition the patient is requested to stare at a black screen, without closing his eyes or making any other ocular movement. The scanning lasts 5 minutes, corresponding to 150 volumes of the entire brain. The voxel size was 2x2x3mm^3,TR=2000 ms and TE=23 ms.

For the task paradigm the subjects had to perform blocks of tasks prompted by a stimulus. The stimuli were displayed visually and required the ability to read. Language tasks include detection of semantic and syntactic errors as well as sentence processing.

Language tasks paradigms consist of:

- Semantical Decision: detection of equals (=) or number signs (#) in the displayed sentences. The sentences were presented according to 3 different frequencies (low, medium, high), composed by two blocks each. Paradigm begins and ends with a rest block.
- Synctatic Decision: 3 tested tasks: gender concordance, temporal conjugation and the correct use of pronouns, each composed of two interleaved blocks. Paradigm begins and ends with a rest block.
- Verb Generation: 4 blocks of linguistic stimuli interspersed with 4 blocks of visual but not linguistic stimui, such as circles and number signs.

For semantic and syntactic paradigms, the number of volumes was 160, whereas for the verb generation paradigm the number was 112. In both paradigms the voxel size

was 2x2x4 TR was 2000ms and the TE was 23 ms .

In respect of motor tasks, these consist of:

- Mouth: 4 task blocks (opening and closing), interspersed with 4 rest blocks. The paradigm begins with the completion of the task.
- Hand: 4 task blocks of hand bilateral motion, interspersed with 4 rest blocks. The paradigm begins with the completion of the task.
- Feet: 4 task blocks of feet bilateral motion, interspersed with 4 rest blocks. The paradigm begins with the completion of the task.

Task acquisitions comprises 80 holocranial volumes, a voxel size of 2x2x4, TR=3000 ms and TE= 33 ms.

3.2 Preprocessing

Data pre-processing was accomplished using a MATLAB® (The MathWorks Inc., MA, USA version R2013a) implemented toolbox called Data Processing Assistant for Resting-State fMRI- advanced edition (DPARSFA) (Chao-Gan and Yu-Feng, 2010). DPARSFA is an user-friendly tool whithin Data Processing and Analysis for Brain Imaging (DPABI) and it is based on some functions in Statistical Parametric Mapping (SPM) (developed by members and collaborator of The Wellcome Trust Centre for Neuroimaging Institute of Neurology, University College London) and Resting-State fMRI Data Analysis Toolkit (REST) (Xiao-Wei Song, 2011). DPARSFA accepts structural and functional data in Digital Imaging and Communications in Medicine (DICOM) format, which is an universal output format of fMRI scans.

The main purpose of this part of the study was essentially to choose the combination of pre-processing parameters that best suited the ultimate goal, which was to recognize and extract task and rest networks. The software template is displayed in fig 3.1.

The pre-processing was performed individually for each subject and one paradigm at a time. Task data and rest data were pre-processed following different pipelines. Below is described pre-processing steps on both cases.

- DICOM to Neuroimaging Informatics Technology Initiative (NIfTI)
  The first step was to convert DICOM files to NIfTI format. This format includes the affine coordinate system, which transforms voxel index (i,j,k) to spatial location (x,y,z) and therefore gives the accurate information about where left and

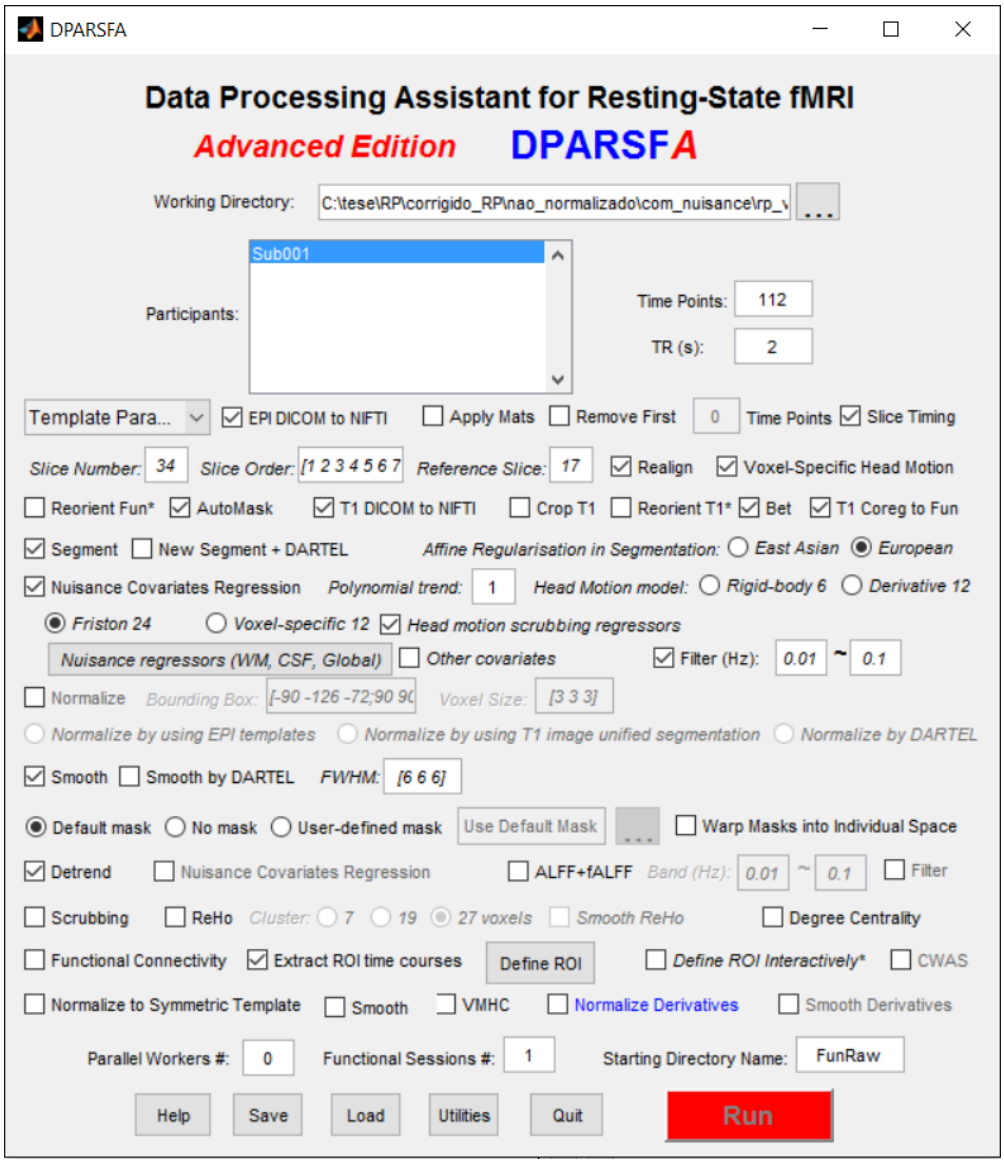

Figure 3.1: DPARSFA layout

right hemisphere is. In DPARSFA functional and structural data are converted independently.

- Remove first time points In the scope of this study, it wasn't required to discard the first volumes since this has already been done as part of the standard acquisition procedure.

- Slice timing This option was checked with the purpose of correcting differences in image acquisition time between slices.

  Slice Number The slice number consists of 38 axial slices acquired continuously for motion paradigms. In semantic, syntactic, verb generation and rest paradigms the number of slices is 34.

  Slice order Slices were acquired one by one from anterior to posterior, from left to right and from bottom to top. Therefore, this option was filled with an array going from 1 to number of slices.

  Reference slice The reference slice was set to the slice acquired at halfway the scan in order to reduce timing corrections.

- Realign - The realignment is applied by rigid body transformations, which assumes that the shape and size of the volumes are the same and that one image can be spatially matched to the first image, which SPM set it as reference, by the combination of three translation (x,y,z; in mm) and three rotation parameters (pitch, roll, yaw; in degrees). These operations are performed by matrices and can then be multiplied together. See equation 3.1. Furthermore, one .txt file is created with each volume's motion specified for each axes and can be further applied as part of nuisance regressor.

$$\begin{bmatrix} 1 & 0 & 0 & X_t \\ 0 & 1 & 0 & Y_t \\ 0 & 0 & 1 & Z_t \\ 0 & 0 & 0 & 1 \end{bmatrix} \times \begin{bmatrix} 1 & 0 & 0 & 0 \\ 0 & cos\Phi & sin\Phi & 0 \\ 0 & -sin\Phi & cos\Phi & 0 \\ 0 & 0 & 0 & 1 \end{bmatrix} \times \begin{bmatrix} cos\Theta & 0 & sin\Theta & 0 \\ 0 & 1 & 0 & 0 \\ -sin\Theta & 0 & cos\Theta & 0 \\ 0 & 0 & 0 & 1 \end{bmatrix} \times \begin{bmatrix} cos\Omega & sin\Omega & 0 & 0 \\ -sin\Omega & cos\Omega & 0 & 0 \\ 0 & 0 & 1 & 0 \\ 0 & 0 & 0 & 1 \end{bmatrix} \tag{3.1}$$

- Voxel-Specific Head Motion The voxel-specific head motion is a nonlinear combination of the positions of the voxels and volume-wise translations and rotations.

Its goal is to minimize the difference of head motion impact on the voxels, depending on their distance from the center of the gradient coil. One text file is created and comprises frame-wise displacements (FD) from the reference image for each volume. This file is further applied in the scrubbing regressor calculation.

- Nuisance Covariates Regression Nuisance signals are those originating from non-neural sources and can cause spurious activations.

  Nuisance regressors Respiration and the cardiac signal are among the sources of those artifactual signals. As these physiological sources are not recorded along with the fMRI scan, it is possible to remove them based upon their frequency. For this purpose nuisance covariates may include global mean signal (respiratory and cardiac cycle), cerebrospinal fluid (CSF) and white matter (WM) signal, figure 3.2. In this study all the covariates mentioned above were regressed out by GLM.

  Head Motion Model In addition to physiological signal regressors, motion regressors were added to GLM model. Those motion regressors included the 6 head motion parameters estimated in the realigment option, plus 6 head motion parameters one time point before, and the 12 corresponding squared items, that are all comprised in Friston 24-parameter model, (Friston et al., 1996 [34]).

  Head motion scrubbing regressors As a final step, head motion scrubbing regressors were generated to be further included in the model. The scrubbing method identifies motion-induced spikes and rejects them based upon a defined FD threshold. Of note that FD were previously estimated on voxel-specific head motion option. In this study, the FD threshold for "bad" time point was 0.5 mm, i.e. all the time points that were displaced 0.5 mm from the first time point considered corrupted. According to the guidelines of Power et al. (2012b), the bad time points as well as 1 before and 2 after neighbours were also excluded from data, figure 3.2. DPARSFA produces one regressor for each time point excluded.

  In conclusion, nuisance covariates removes physiological, non-neuronal noises from data, and produces a matrix of regressors (or covariates) where each line characterizes one time-point, and each column represents 24 motion parameters, plus WM, CSF and global mean signal, and an undefined number of scrubbing regressors.

Nuisance Covariates Regression is mentioned in the literature as being an ideal method for pre-processing rest data [55]. Its contribution was tested in the final

results and its application or not as preprocessing stage was analyzed.

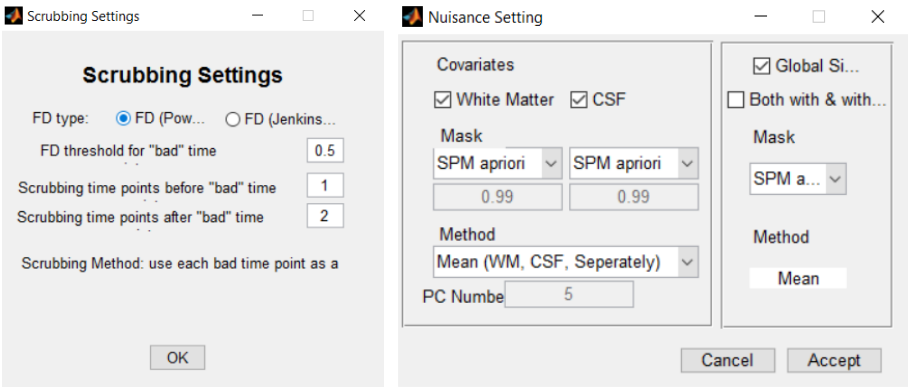

a Scrubbing Settings b Nuisance Settings

Figure 3.2: DPARSFA options

- brain extraction tool (BET) BET was used to remove non-brain areas.

- Normalize The acquisition of fMRI images may vary depending on the intended purpose. Thus the position, angle and dimensions of the images obtained are specific for each paradigm. So that images become comparable it is essential that all of them are normalized to the same space. Normalize function is used to put scans into Monreal Neurological Institute (MNI) space. This function understates the differences between two scans by minimizing the sum of squares of intensity differences. The normalization can be based on the standard template (MNI), however in subject-specific studies, as the present study, it is preferable to use the patient's anatomical images as a template. Voxel size that best fits the data of this study was [3 3 3] and bounding box's measures were specified by SPM itself. Normalize option requires co-registration and segmentation.

  Segment Segment separates grey matter, white matter, and CSF in anatomical images.

  Structural Coregistration to Functional Coresgistration aligns functional images into the same space and orientation of anatomical ones. Besides, any transformations in structural data can be applied in functional images.

- Smoothing Spatial smoothing was performed in this study in order to filter out high-frequency spatial noise and thereby improve signal-to-noise ratio, as well

as make the data more complying with the specifications of the underlying statistical theory (Gaussian Random Fields). This was accomplished by convolving the images with a Gaussian kernel. In order to achieve the best pre-processing pipeline, several kernel sizes were tested. From the matched filter theorem, the best kernel size is about the same size as data activation. As it wasn't known, at the pre-processing stage, the precise size of activations, although it was known that they wouldn't be much significant, the size of the Gaussian that best suited the study's interest was a small one with full width at half maximum (FWHM) of 6 mm, which is in concordance with previous studies and follows a well-established rule of thumb that suggests that the kernel width should be about 2 to 3 times voxel size.

- Filter Temporal filtering was performed by a 0.01- 0.1 Hz bandpass filter, removing low-frequency drifts and physiological high-frequency respiratory and cardiac signals.

- Detrend Several studies demonstrated the importance of removing linear trends in voxel time courses in individual subjects. The origin of these trends is not completely understood, but they occur due to long-term physiological shifts. DPARSFA relies on REST to estimate the linear trends with a least-square fitting of a straight line, which is removed from the data. Subsequently, the original mean value of each time course is added back.

- Scrubbing To save computational time, scrubbing option was not performed in pre-processing stage, since it was previously included as a regressor on nuisance matrix.

3.3 Processing

Task data was processed whith SPM, while rest data was processed with Group ICA of fMRI toolbox (GIFT).

3.3.1 Task data - Statistical Analysis

In order to reliably detect voxels activated by task paradigms, statistical data analysis was performed by GLM in SPM, consult subsection 2.2.4.3.

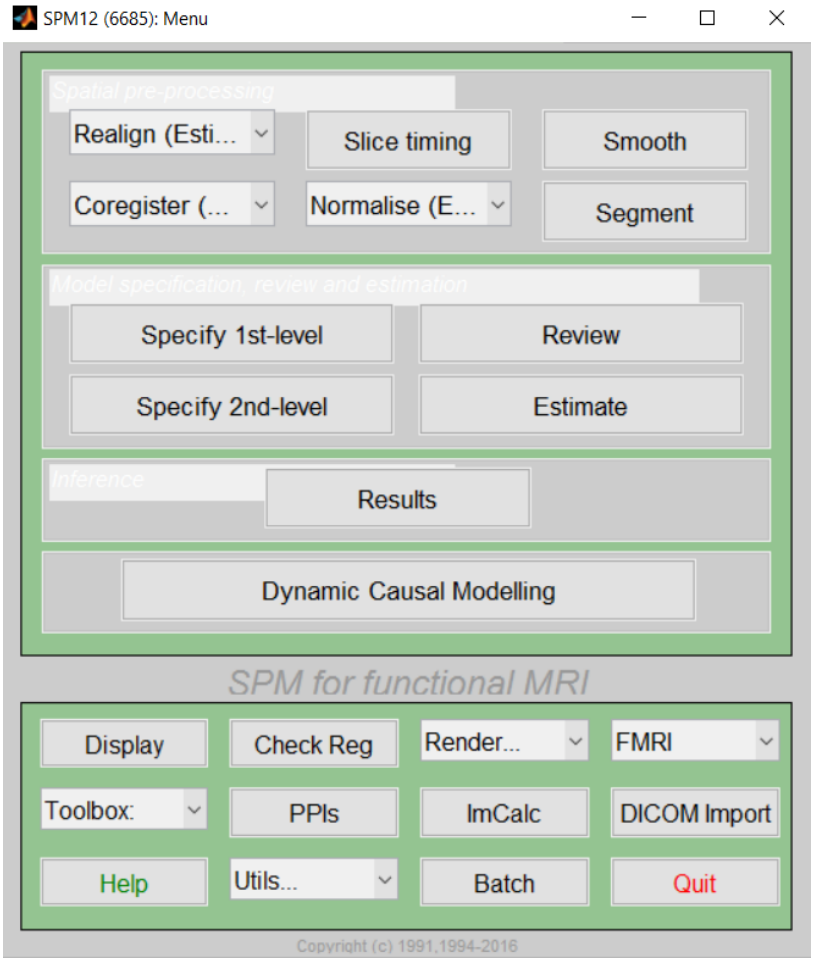

Figure 3.3: SPM layout

3.3.1.1 Model specification

GLM identifies the areas with significant BOLD signal change, induced by cognitive tasks. For that purpose the signal model was constructed by convolution of canonical hemodynamic response function (hrf) with the boxcar function of each task, including the pre-processing nuisance regressors. Both hrf and model regressors were designed based on scan numbers, i.e., the first scan corresponds to timepoint zero and the second one corresponds to timepoint 1, and so on. The time between the start of sequential scans, or interscan interval, was established based upon TR (2s for linguistic paradigms and 3s for motion paradigms).

As the purpose of this study was subject-specific analysis, the model specification was accomplished by a first level design, therefore each session only models one task

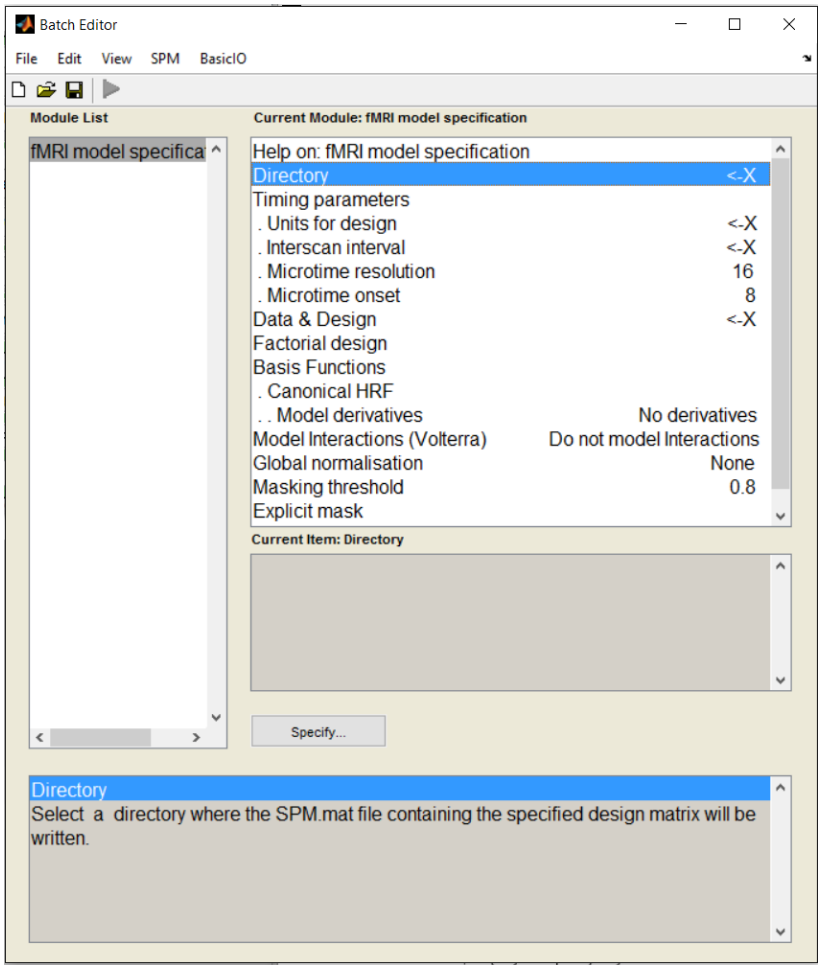

Figure 3.4: fMRI model specification

paradigm for one subject. In the context of feet, hands, mouth and verb generation paradigms, only one boxcar condition was defined per session, since those cases reflected on-off stimulation paradigms. On the other hand, 4 conditions were setted for each semantic and syntactic task. As regards to semantic decision, the 4 conditions describe the 3 frequencies of the stimuli (low, medium, high) and the free-stimulus condition at the beginning and end of the task. Relatively to syntactic decision, the 4 conditions were gender concordance, temporal conjugation an correct use of pronouns, including the free-stimulus condition at the beginning and end of the task. The onset times and the period of the stimulation were specified in the SPM framework.

As regards to other predictors to be implemented, two distinct processes were followed depending on whether pre-processing included nuisance covariates regression

or not. In the first case, a multiple regression was performed resorting to nuisance covariates matrix created in the pre-processing stage. On the other hand, head motion regressors were included in the model through realignment parameters' text file and an additional regressor in cases where the subject performed to much movement. The latter array was created using MATLAB® functions and attempted to reproduce head motion scrubbing regressor. For this purpose, the construction of the array resorted on the framewise displacement of each volume. If the displacement was higher than 0.5 mm then that volume, such as the one before and the two after adjacent volumes were excluded, ie were represent by an '0' in the vector. The remaining volumes acquire the value '1'.

Masking data aims to only estimate voxels that seem to have significant signal in them. As for the default SPM sets masking threshold threshold to 0.8, which means that the model is estimated based on voxels whose mean value is at 80% of the global signal. However if nuisance covariates regression formed an integral part of the pre-processing, this threshold has to be setted to -inf. As the significance of the activation voxels is low, mask that include all brain, and not a specific portion, was applied.

3.3.1.2 β estimation and contrast

After the model be established, GLM estimated β values using an autoregressive model during restricted maximum likelihood (ReML) parameter estimation, which assumes that each voxel has the same error correlation structure.

Once β were estimated, we tested if the most significant β were assigned to the most important regressors of the model, in other words, if the most important regressor was greater than 0. Within the context of this experiment, the most important regressors were the ones that describe the defined conditions. To test that, we relied on GLM T-contrasts to define the hypothesis and t-test to assess it.

In GLM, a contrast specifies linear combinations of β. In motion paradigms context, as only one on-off condition was defined for each motion, a simple contrast was applied.

$$\begin{bmatrix} 1 & 0 & 0 & \cdots & 0_n \end{bmatrix}$$

Where n is the number of regressors.

In the case of semantic and syntactic paradigms, a weighted contrast between the different conditions, plus a -1 weighted, to ensure that the sum of weights was zero, was established, like the following array.

$$\begin{bmatrix} 0 & \frac{1}{3} & \frac{1}{3} & \frac{1}{3} & -1 & 0 & \cdots & 0_n \end{bmatrix}$$

Finally in verb generation, where the model responses to two conditions (verb generation + baseline), a [1,-1] contrast was established to compare the two conditions. Hence, the second β was subtracted to the first before it was tested against zero, i.e, $\beta_1 - \beta_2 > 0$.

After defining t-contrasts, SPM performed a t-test, which estimated t values for the whole brain by calculating the ratio of the contrast of the estimated paradigms by the deviation of variance, equation 3.2.

$$t = \frac{\text{contrast of estimated parameters}}{\sqrt{\text{variance estimate}}} \Leftrightarrow t = \frac{c'\beta}{\sqrt{s^2 c'(X'X)c}} \tag{3.2}$$

At last, several p-thresholds (corrected and uncorrected) were assessed for each task of each participant, in order to maximize the number of true positives while reducing the false ones.

3.3.2 Rest data processing

For rest data processing, the adopted approach was to replicate the procedures used in relevant studies, namely Sair et al. and Tie et al. Therefore, the resting state data was processed through Independent Component Analysis by GIFT. The software template is displayed in figure 3.5.

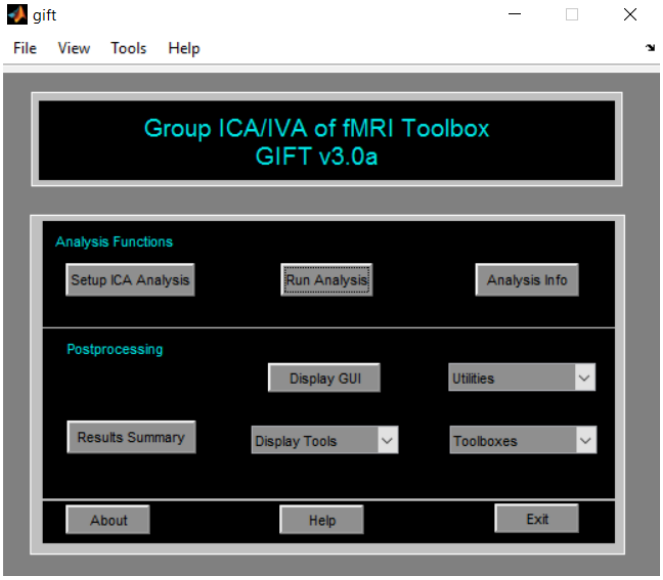

Figure 3.5: GIFT layout

Just like the studies mentioned above, components were estimated for each subject using the minimum description length (MDL) criteria. ICA maps were generated for 20 and 50 independent components using Infomax algorithm. In order to determine the reliance and stability of the previously selected ICA algorithm, ICASSO toolbox was applied. ICA algorithm ran 5 times, and each run started with a different initial value (RandInit), figure 3.6.

The extracted independent components were then visually assessed using the software display option, figure 3.6

.

3.4 Comparison of Task Networks and Resting State Networks

In order to evaluate how rest activation maps are related to task activation maps, different similarity coefficients were employed. The precedent procedures that characterize this analysis are described below.

For each task of each participant, 4 different activation maps were created in SPM. Each map resulted from the application of the following different significance levels:

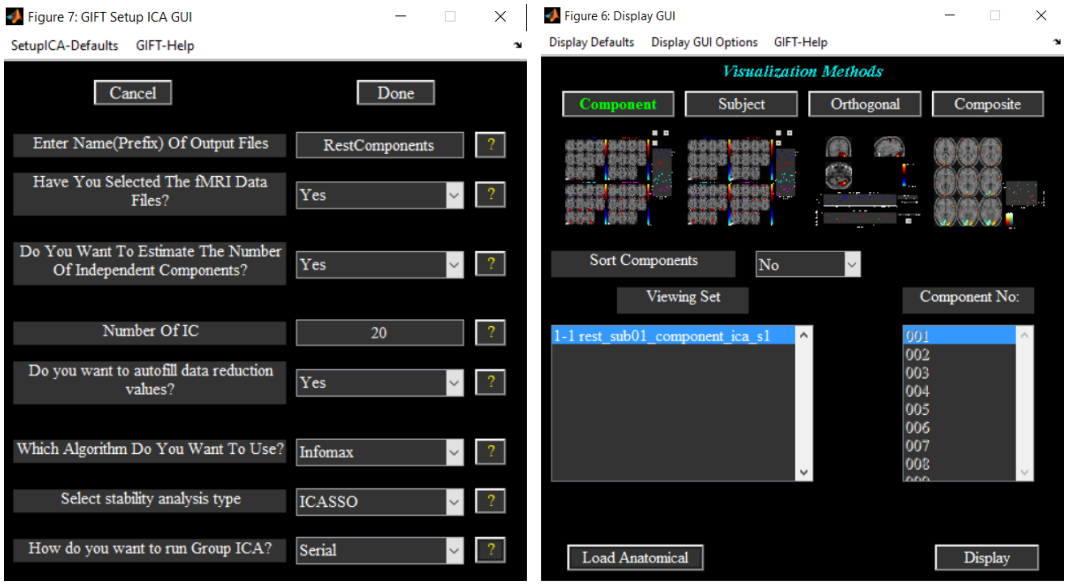

a ICA model specification b GIFT display GUI

Figure 3.6: GIFT options

- FWE 0.05;
- FWE 0.01;
- FWE 0.1;
- Uncorrected 0.001.

Activation maps for task paradigms were then binarized using an option provided by SPM, allow to obtain a 3D image in nifti format, where 1 represents the significant activations for the selected p-value. The binarization step is essential to implement the similarity coefficients, as will be explained later in this section.

In the meantime, binarization of the rest activation maps was achieved by using 9 intensity thresholds, applied to each independent component previously extracted in the GIFT software. These thresholds varied between 10% and 90% of the total's intensity, with an increment of 10% between each.

The resemblance between the binarized images was subsequently calculated with 3 different coefficients. The first one, which is one of the most used, is the Dice similarity coefficient (DSC) and it is described by the equation 3.3.

$$DSC = 2\frac{|R \cap T|}{|R| + |T|} \tag{3.3}$$

The numerator is the overlap between the activations of rest (R) and task (T) binarized maps, and the denominator is the sum of both.

This coefficient takes values between 0 and 1, wherein 1 is the perfect overlap, whereas 0 describes the opposite event. A low value of the DSC can represent one of two situations: the intersection of rest and task activations is low or the union between the two activations is high. As the reason why Dice coefficient might be low can not be directly measured by this index it became necessary to create two more indexes.

One of them, equation 3.4, is a measure of the overlap of rest activation maps on task activation maps, ie, if the index has the value 1, means that all task activations match rest activations, however does not directly imply that all the rest activations coincide with task activations. This coefficient, will be henceforth designated by Similarity Coefficient 1 (or SC_1).

$$SC_1 = \frac{|R \cap T|}{|T|} \tag{3.4}$$

Lastly, equation 3.5 attempts to find the contribution of rest activations in the overlap of the two maps. This coefficient, will be hereinafter designated by Similarity Coefficient 2 (or SC_2). If this index is close to 1 it means that there are no coincidences on where the rest and task activations take place.

$$SC_2 = \frac{\left|R \cap \overline{T}\right|}{|R|} \tag{3.5}$$

The next scheme aims to lay out some of the most important steps in pre-processing, processing, and data analysis.

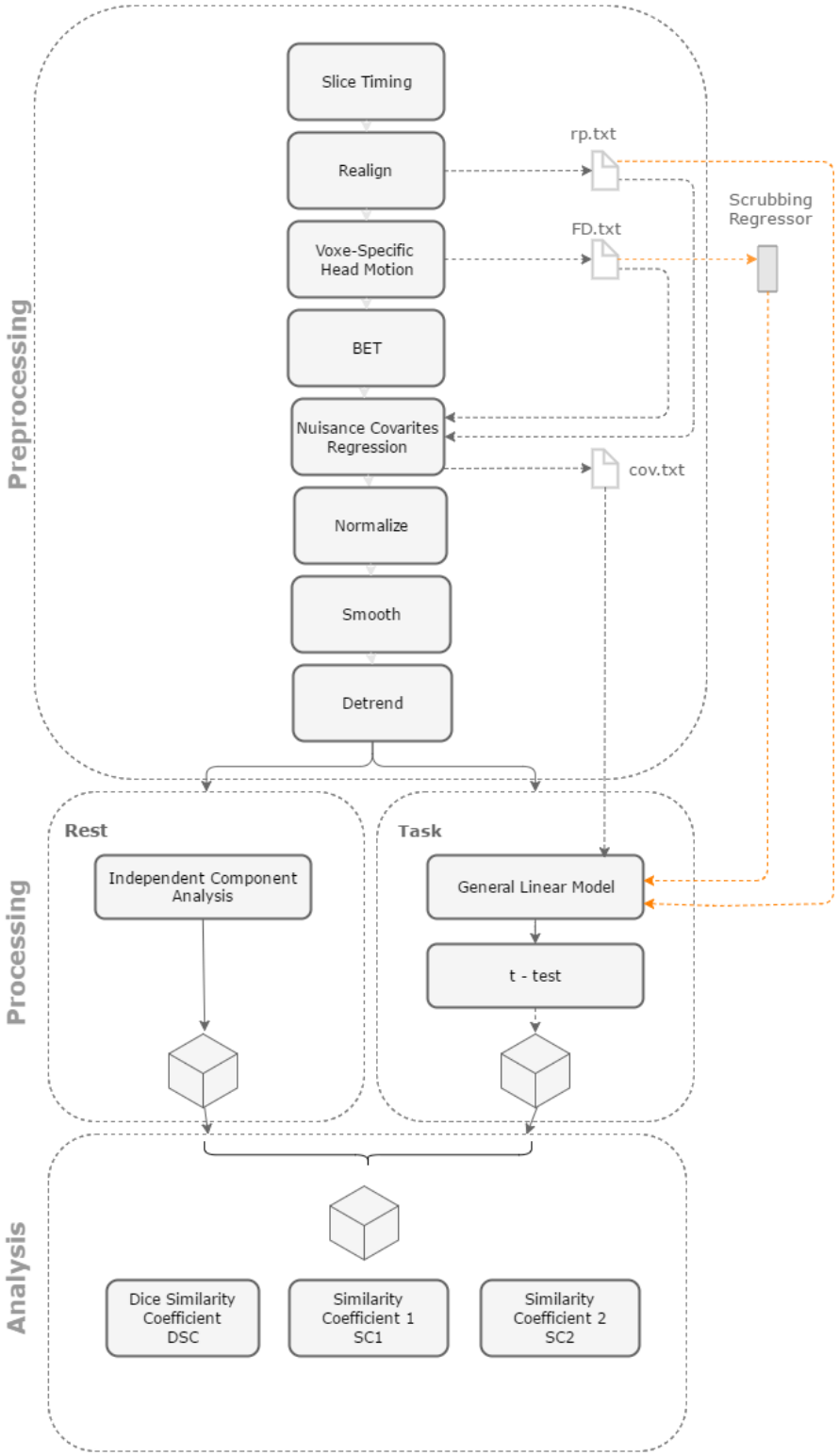

Figure 3.7: The overall scheme

Chapter 4

Results

This chapter is intended to report the most relevant results obtained in pre-processing and processing stages, followed by the presentation of statistical and similarity analysis results. Due to the large volume of data, results from the latter will be presented in two different approaches. One intends to present the outcomes of all tasks for a single participant, and the other approach aims to present the results of one single task for all subjects. The selection criterion of the subject and task to present in this section is the minimum number of volume removed by the scrubbing procedure.

4.1 Important results from preprocessing

As the design of a preprocessing protocol was a key part of this research, herein are the results of some of the parameters which arouse more questions.

4.1.1 Scrubbing

The amount of volumes removed by scrubbing method is presented in the table 4.1. It is important to emphasize that the volumes presented in the chart comprise the ones that have a framewise displacement greater than the value stipulated by Power et al. [56] as well as the preceding volume and the following two. They were regressed out from a total of 80 volumes in motor paradigms, 160 in semantic and syntactic decision, 112 in verb generation and finally 150 in rest.

From the information presented in the table, it is possible to affirm that subject 003 is the one with fewer volumes removed, alongside with Sub006. For the first one, only hands motor paradigm led to a framewise displacement greater than the value stipulated by Power et al., while in the second one volumes were withdrawn only in the syntactic decision. Subject 005 is the one with the largest number of volumes removed, since in all tasks, and rest included, several volumes had to be regressed out. Another finding worth mentioning is the major impact of scrubbing on language paradigms for subject 001 and 002, since only 10 time points remain in each paradigm.

Regarding to tasks, the feet paradigms are noted for producing the largest number of removals between the motor tasks, while the semantic decision stands out among the linguistics. In rest, few or none volumes were removed, excepting for Sub005.

Table 4.1: Scrubbing Results

Subject ID	**Motor Paradigms**			**Linguistic Paradigms**			**Rest**
	Mouth	Hands	Feet	Semantic Decision	Syntactic Decision	Verb Generation	
Sub001	0	10	0	150	150	150	0
Sub002	4	0	34	150	150	150	4
Sub003	0	4	0	0	0	0	0
Sub004	14	0	0	0	0	0	0
Sub005	55	51	62	150	85	30	56
Sub006	0	0	0	0	13	0	4
Sub007	0	0	12	0	4	0	4
Sub008	0	4	0	36	9	27	4

4.1.2 Normalization

As mentioned in section 3.2, the image acquisition is different for motor tasks and for rest and language tasks. This difference is more evident in the images dimensions. The dimensions of motor tasks images are 128x128x38 while rest and language tasks images have a dimension of 128x128x34, which results in an inconsistent comparison and in the impracticability of similarity analysis between the motor tasks data and rest. To illustrate this difference, the figure 4.1 contains a representation of mouth task image and semantic decision of Sub003 immediately before and after normalization to Montreal Neurological Institute (MNI) space.

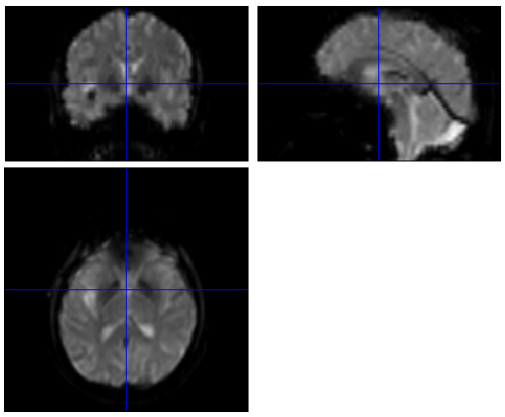

a Mouth task, immediately before normalization

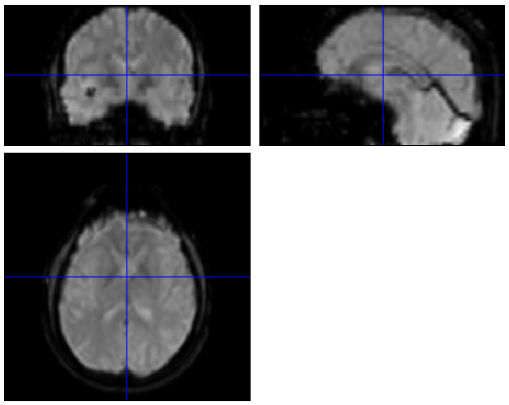

b Semantic Decision, immediately before normalization

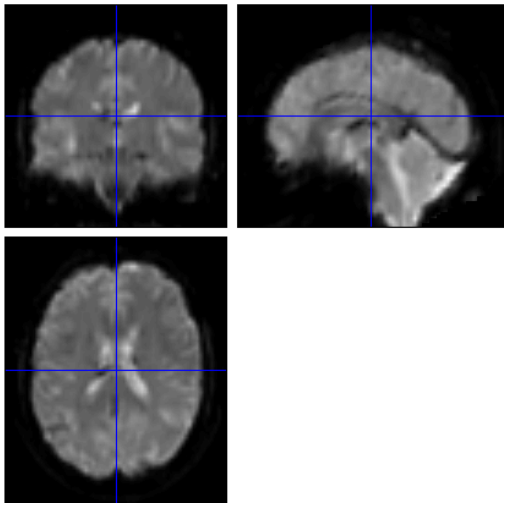

c Mouth task, immediately after normalization

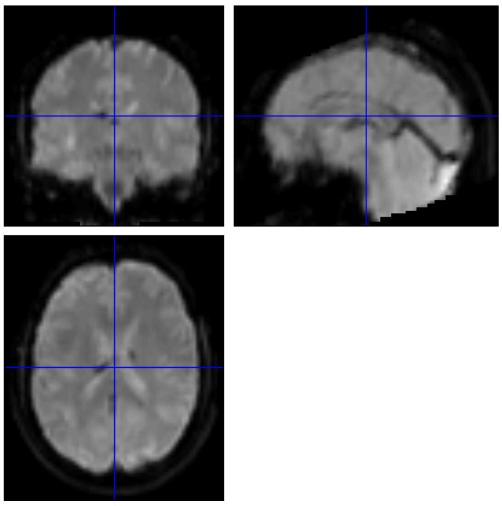

d Semantic Decision, immediately after normalization

Figure 4.1: Difference between normalize and not normalize images. The upper images represent the paradigm of the mouth and semantic decision before being normalized to the MNI space, while the bottom ones are the same paradigms after normalization. These images belong to the subject under review, Sub003. Adapted from SPM.

4.1.3 Removal of nuisance signals

The removal of the nuisance signals includes removing all non-neuronal signals and produces the visual effect illustrated in fig 4.2. The sub figure related to the performance of this procedure is much more blurred than one that not contemplates it.

Despite the removal of nuisance signals produce an overly blur effect it is not automatically indicative of a worse activations extraction. Thus, to test the efficiency of this procedure two analysis were carried out in parallel, one using this procedure and the other not. The results of these two analysis are available in section 4.2.1.1.

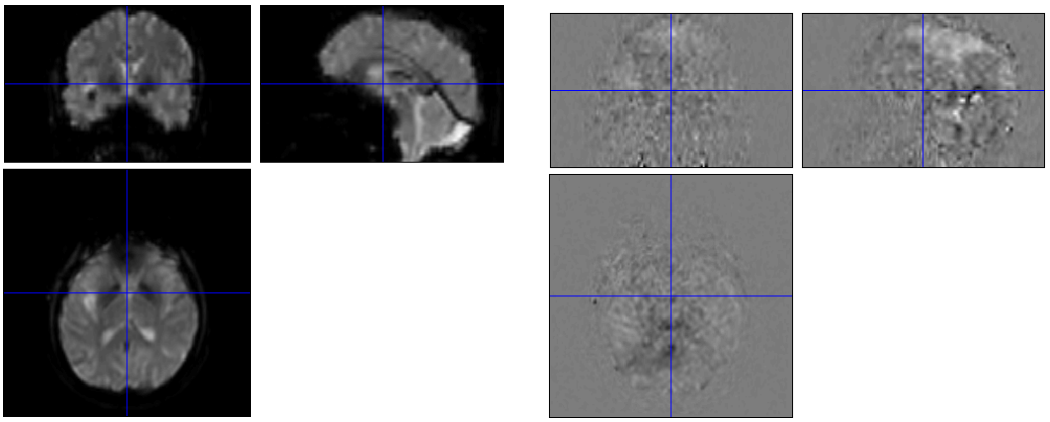

a Mouth task, immediately before removing nuisance signal

b Mouth task, immediately after removing nuisance signal

Figure 4.2: Effect of nuisance signals removal. These images belong to the subject under review, Sub003. Adapted from SPM.

4.2 Intra-Subject Analysis

This section aims to present the results in an intra-subject perspective. Thus, the results of activations mapping of all task paradigms and at rest will be presented for subject 003. The choice of this subject, as mentioned earlier in this chapter, is related to the small number of volumes removed by scrubbing (consult table 4.1).

4.2.1 Motor Paradigms

4.2.1.1 Mouth paradigms

As described in section 3.4, similarity tests were conducted by resorting to 4 distinct maps coming from Statistical Parametric Mapping SPM. Each map results from a different significance level. The visual effect of selecting different p-values can be found in figure 4.3.

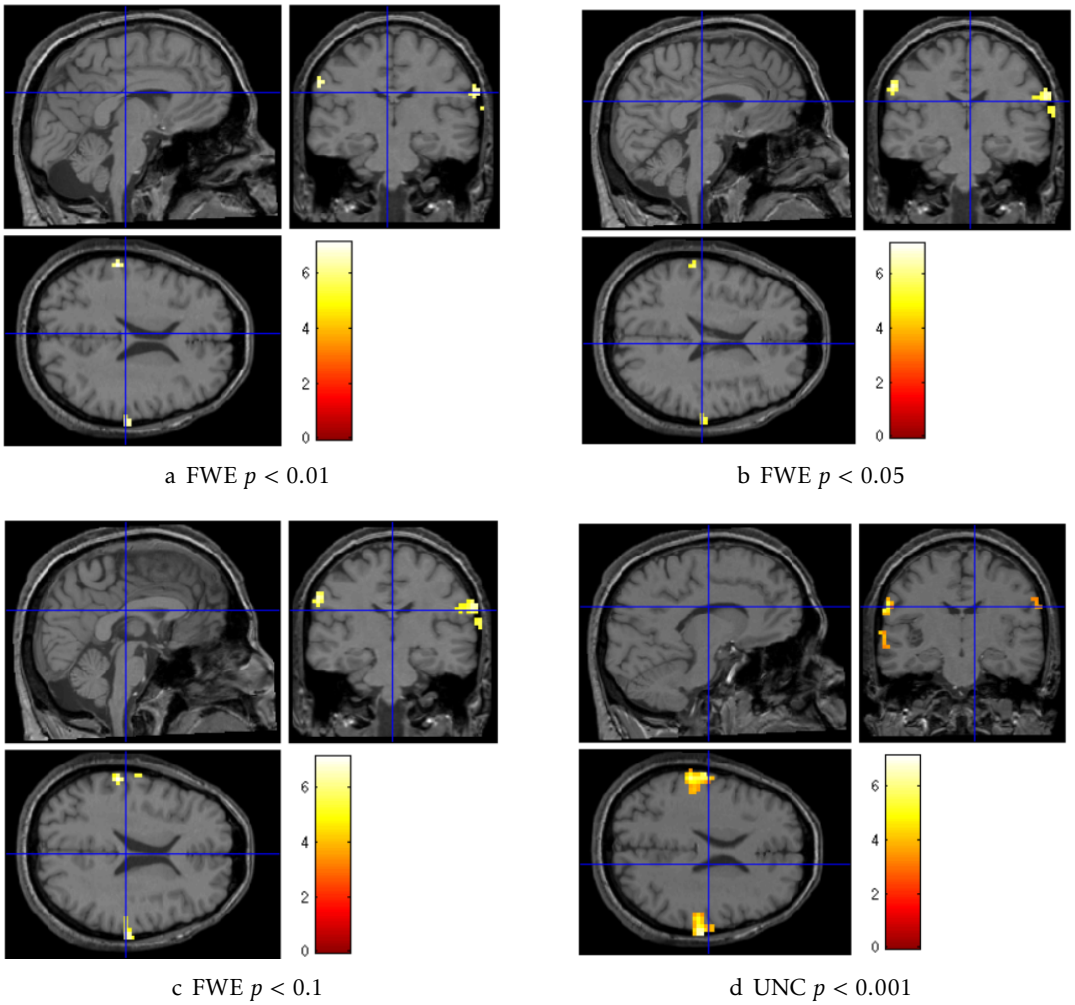

a FWE $p < 0.01$ b FWE $p < 0.05$

c FWE $p < 0.1$ d UNC $p < 0.001$

Figure 4.3: SPM activations map resulting from mouth paradigm of Sub003. Each map represents the activation using a distinct p-value. Mouth activation with a) p-value inferior to 0.01 FWE; b) p-value inferior to 0.05 FWE c) p-value inferior to 0.1 FWE; d) p-value inferior to 0.001 uncorrected;

The first three images are listed in ascending order of p-values with familywise error FWE correction (FWE), whereas the image at the bottom right has an uncorrected p-value of 0.001. For more conservative levels of significance the number of activations is smaller than in the case where no corrections were performed along with the statistical tests.

SPM displays images in neurological convention, which means that the left side of

the image corresponds to the left side of the brain. In this specific case, functional images were superposed with structural images specific to the subject, in order to improve the perception of regions where activations take place.

From the figures it is clear that there is bilateral activation in the ventral portion of the precentral gyrus, immediately above the Sylvian fissure. Additionally, in the bottom right image it is possible to distinguish an activation below the Sylvian fissure. SPM enables the visualization of the activations, as well as presents the designed model and a table with the relevant statistical values, figure 4.4. Among other information, the table presents the statistical significance of voxel intensity ("peak level"), which was the approach used in this study, but also presents the statistical values related to cluster extent ("cluster level") and a global p-value related to the whole map which combines intensity and extent information and reflects the likelihood of getting the activation pattern by chance ("set level"). Uncorrected p-values are shown alongside p-values corrected using FWE and False Discovery Rate (a less strict method).

From the 50 independent components extracted by the Group ICA of fMRI toolbox, GIFT software, the 5 wich most resemble task activations were selected. Thereunto, one correlation map between the binarized activation maps of all independent components and task activation maps was used to infer the most relevant components for the study. This procedure was repeated for each p-value activation map for each similarity test, accounting for a total of 12 colormaps for each task.

Taking the example highlighted in this section, and considering only the correlation map in the case of a p-value < 0.05 (FWE) and the Dice similarity coefficient (DSC) test, the most significant independent components for mouth motion paradigm were IC number 33, 21, 50, 19 and 3, as shown in figure 4.5.

In order to ensure a proper analysis of the data, the maps of the most important independent component (IC) were visually evaluated, figure 4.6. The image was directly extracted from the GIFT environment, whereat it not reflects the intensity threshold that was applied to it.

The figure consists of several transverse planes of the brain ordered from superior planes to inferior ones. In the superior planes, activations are located over the coronal plane. As the planes become more inferior, activations emerge in the sagittal plane and for planes even further inferior activations become bilateral. Along planes it is possible to evidence the existence of residual activations scattered throughout the brain.

Figure 4.4: SPM environment. In the upper left corner, there is the map of activations. In the upper right corner is displayed the designed model matrix.And in the bottom of the image is presented the statistical table

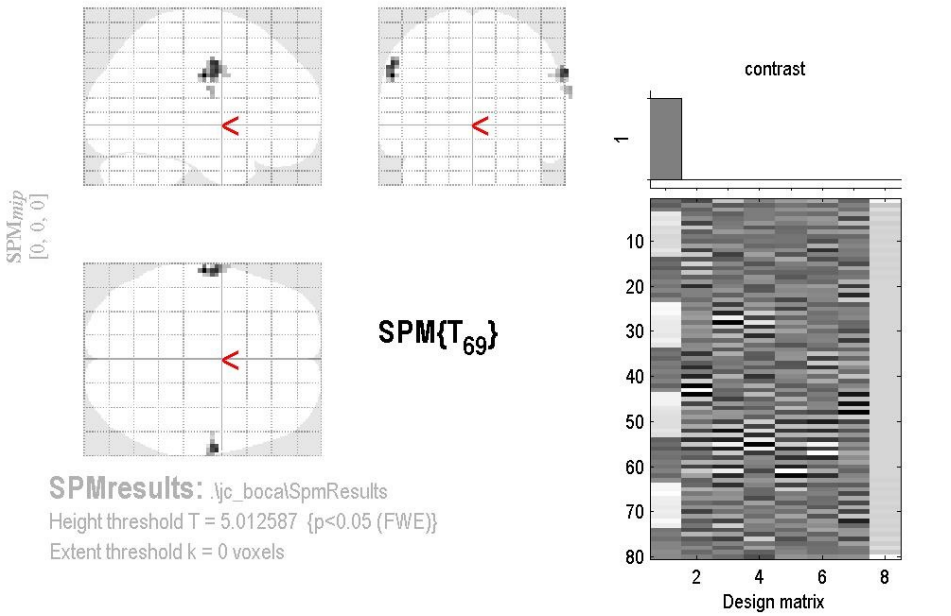

Statistics: ***p-values adjusted for search volume***

set-level		cluster-level				peak-level					mm mm mm
p	*c*	$p_{FWE\text{-}corr}$	$q_{FDR\text{-}corr}$	k_E	p_{uncorr}	$p_{FWE\text{-}corr}$	$q_{FDR\text{-}corr}$	*T*	$(Z_{=})$	p_{uncorr}	
0.000	3	0.000	0.005	36	0.002	0.000	0.004	7.13	6.15	0.000	-60 -15 33
						0.000	0.007	6.66	5.83	0.000	-60 -6 42
						0.015	0.353	5.37	4.89	0.000	-63 3 33
		0.001	0.023	19	0.015	0.000	0.007	6.68	5.84	0.000	66 -6 36
						0.024	0.466	5.25	4.79	0.000	54 -9 33
		0.005	0.094	8	0.094	0.008	0.218	5.57	5.04	0.000	69 -12 24

table shows 3 local maxima more than 8.0mm apart

Height threshold: T = 5.01, p = 0.000 (0.050)
Extent threshold: k = 0 voxels
Expected voxels per cluster, <k> = 2.935
Expected number of clusters, <c> = 0.05
FWEp: 5.013, FDRp: 6.477, FWEc: 8, FDRc: 19

Degrees of freedom = [1.0, 69.0]
FWHM = 14.4 14.3 14.0 mm mm mm; 4.8 4.8 4.7 {voxels}
Volume: 1942785 = 71955 voxels = 607.7 resels
Voxel size: 3.0 3.0 3.0 mm mm mm; (resel = 106.57 voxels)

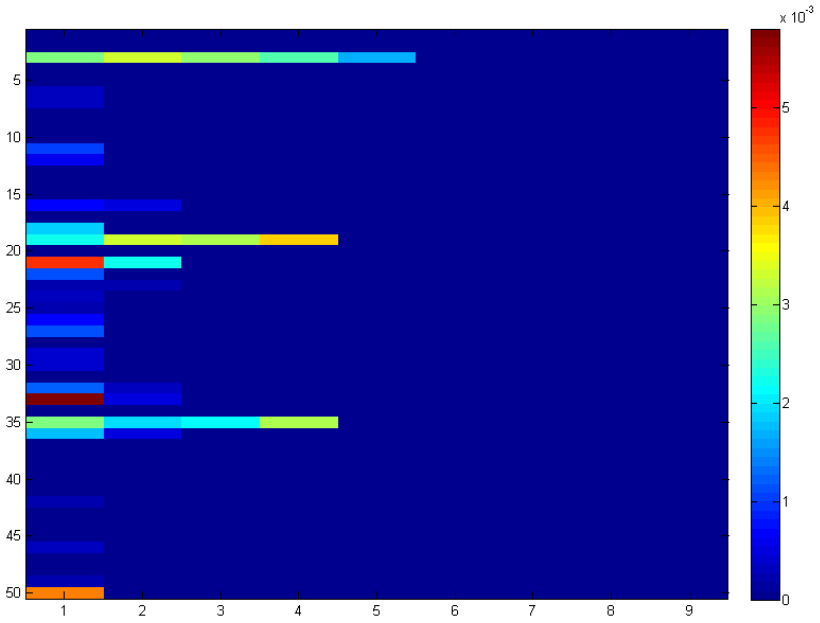

Figure 4.5: Correlation map of IC extracted from rest data with different intensity thresholds, for mouth activation map of Sub003, with a p-value < 0.05 FWE. The y-axis represents each of independent components and the x-axis is the intensity threshold, with 1 corresponding to 10% and 9 corresponding to 90% of maximum intensity. The most significant IC are 3, 21, 50, 19 and 3.

The results of the similarity tests between resting-state and task activation maps are displayed in table 4.2. Due to the high amount of data, the results presented in the table expound the 5 best outcomes. Dice Similarity Coefficient(DSC) has the lowest correlation values among the 3 similarity coefficients, whereas the Similarity Coefficient 2 has the highest outcomes. In a general overview, the similarity values of DSC increase for p-values less conservative, while SC_1 and SC_2values decrease. The increase in DSC values means that the performance of too restrictive statistical thresholds leads to the removal of activated task regions that are coincident with the activated regions in resting state. The decline in the latter coefficients derives from the increased activated mouth regions as result of application of a low restrictive statistical threshold.

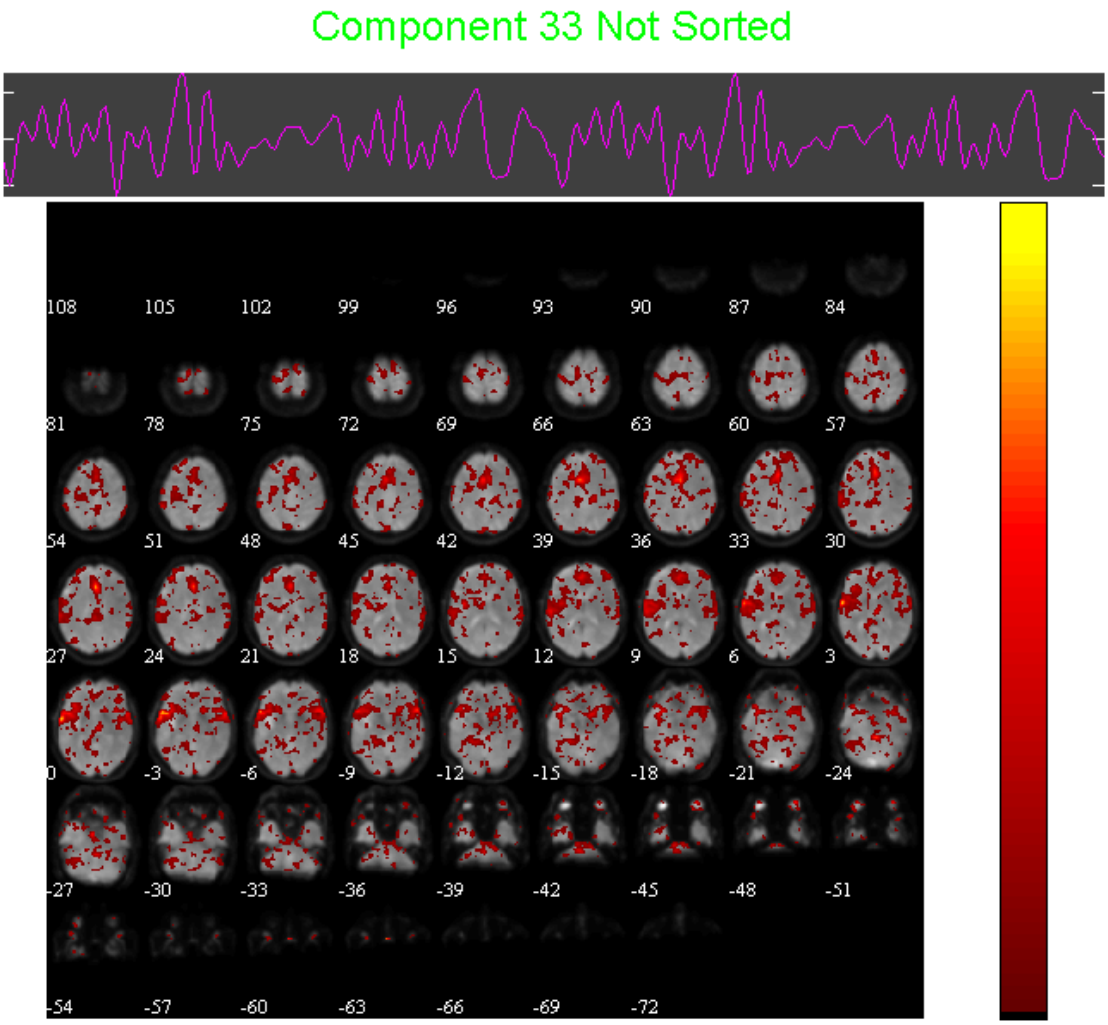

Figure 4.6: Independent Component of Sub003 rest network obtained in GIFT software. The figure consists of several transverse planes of the brain ordered from superior planes to inferiors.

Table 4.2: Similarity results for rest activation maps and mouth paradigm activation maps for Sub003.

	IC	Intensity Threshold	DSC (max)	IC	Intensity Threshold	SC1 (max)	IC	Intensity Threshold	SC2 (min)
FWE 0.01	33	0.1	0.0032	33	0.1	0.8387	33	0.1	0.9984
	50	0.1	0.0025	50	0.1	0.7742	50	0.1	0.9987
	21	0.1	0.0023	3	0.1	0.6774	21	0.1	0.9989
	3	0.2	0.0018	35	0.1	0.5484	3	0.2	0.9991
	3	0.3	0.0017	3	0.2	0.5161	3	0.3	0.9992
FWE 0.05	33	0.1	0.0058	33	0.1	0.7619	33	0.1	0.9971
	21	0.1	0.0048	50	0.1	0.6508	21	0.1	0.9976
	50	0.1	0.0043	3	0.1	0.6191	19	0.4	0.9978
	19	0.4	0.0039	35	0.1	0.5714	50	0.1	0.9978
	3	0.2	0.0032	3	0.2	0.4762	19	0.2	0.9983
FWE 0.1	19	0.3	0.0076	33	0.1	0.7342	19	0.4	0.9956
	33	0.1	0.0070	50	0.1	0.670.9	33	0.1	0.9965
	19	0.4	0.0061	35	0.1	0.5696	19	0.3	0.9967
	19	0.2	0.0060	3	0.1	0.5443	19	0.2	0.9969
	50	0.1	0.0056	3	0.2	0.4177	50	0.1	0.9972
UNC 0.001	19	0.3	0.0357	35	0.1	0.5318	33	0.7	0.9706
	19	0.4	0.0301	33	0.1	0.5202	19	0.4	0.9734
	19	0.2	0.0249	50	0.1	0.4884	33	0.5	0.9736
	35	0.4	0.0226	3	0.1	0.4711	33	0.6	0.9762
	21	0.1	0.0221	21	0.1	0.3150	19	0.3	0.9771

- **Similarity test without nuisance signals**

  All procedures described above were repeated for the data from the nuisance signal removal. The overall result of the similarity tests are shown in table 4.3.

  For the most restrictive threshold of p-value, no value of DSC was greater than 0. This outcome stems from a null intersection of task and rest activations maps, which may mean not only that activations do not overlap as at least one of the maps does not include any activation. As regards to the SC_1, all the results were an indeterminate form $\frac{0}{0}$, which means that the applied statistical threshold was too severe, and no activation remained in the task map. Finally, no SC_2 was different from 1 thus ensuring the existence of activations at rest.

  As for the others p-values, the results express the same pattern verified in data with nuisance signals, namely the very low values of DSC and very high values of SC_2. The maximum value observed in some cases of SC_1, results from the absolute overlap of the rare regions activated in the task with rest areas.

As the results obtained with the extraction of nuisance signals proved to be worse than the ones which arises from images within nuisance signals, study was conducted using only the latter.

Table 4.3: Similarity results for rest activation maps and mouth paradigm activation maps for Sub003, with nuisance signals removal.

	IC	**Intensity Threshold**	**DSC (max)**	**IC**	**Intensity Threshold**	**SC1 (max)**	**IC**	**Intensity Threshold**	**SC2 (min)**
FWE 0.01	0			-			1		
FWE 0.05	42	0.1	0.0003	18	0.1	1.0000	42	0.1	0.9998
	18	0.1	0.0002	28	0.1	1.0000	18	0.1	0.9999
	43	0.1	0.0002	42	0.1	1.0000	43	0.1	0.9999
	28	0.1	0.0001	43	0.1	1.0000	28	0.1	0.9999
	-	-	-	-	-	-	-	-	-
FWE 0.1	18	0.3	0.0015	18	0.1	1.0000	18	0.3	0.9992
	18	0.2	0.0012	6	0.1	0.8000	18	0.2	0.9994
	18	0.1	0.0009	45	0.1	0.6000	18	0.1	0.9995
	36	0.1	0.0006	18	0.2	0.4000	36	0.1	0.9997
	6	0.1	0.0006	28	0.1	0.4000	6	0.1	0.9997
UNC 0.001	18	0.2	0.0116	18	0.1	0.3072	18	0.2	0.9939
	18	0.1	0.0093	19	0.1	0.1867	18	0.1	0.9953
	18	0.3	0.0080	6	0.1	0.1687	18	0.3	0.9955
	36	0.1	0.0078	25	0.1	0.1687	22	0.3	0.9959
	40	0.1	0.0071	45	0.1	0.1687	40	0.3	0.9959

The procedure performed to test similarity between resting-state networks and mouth paradigm networks was reproduced for the remaining 5 tasks.

4.2.1.2 Hand

The results of applying different statistical thresholds to the paradigm hand data is represented in the figure 4.7.

As in mouth activation maps, for more restrictive p-values and its correction, the number of activations is smaller than in the case where no corrections were performed along with the statistical tests. The activation is bilateral, with a clear dominance of the right hemisphere since its expression is evident for less restrictive statistical corrections. The activation area emerged in the upper regions of precentral and postcentral gyrus.

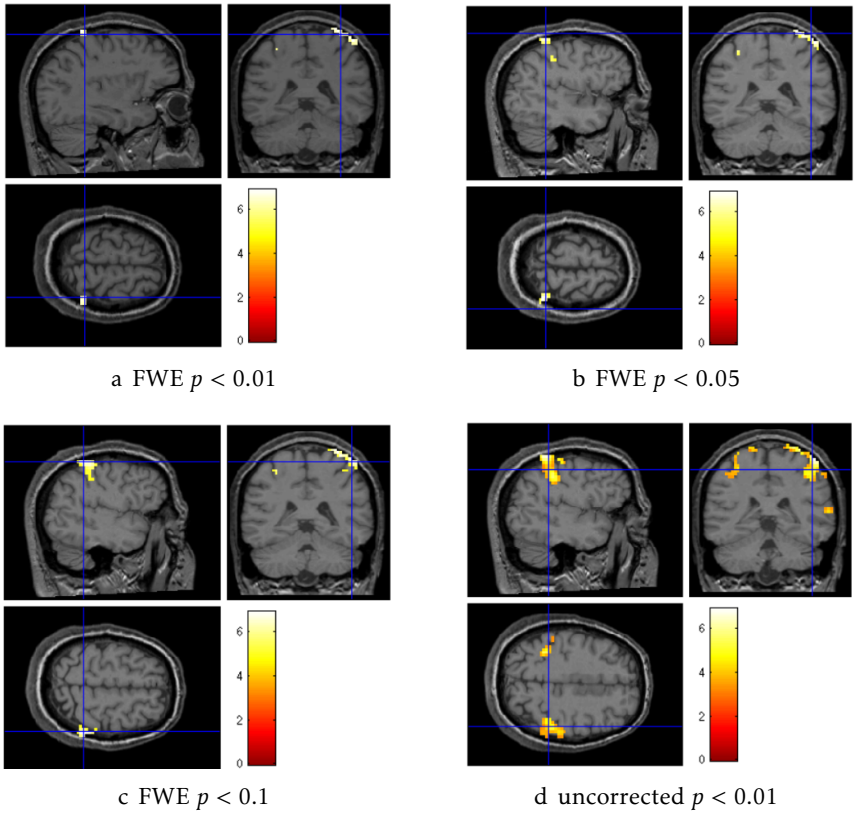

a FWE $p < 0.01$ b FWE $p < 0.05$

c FWE $p < 0.1$ d uncorrected $p < 0.01$

Figure 4.7: The 4 images at the top represent mouth activation with distinct p-values a) p-value inferior to 0.01 FWE; b) p-value inferior to 0.05 FWE; c) p-value inferior to 0.1 FWE; d) p-value inferior to 0.001 uncorrected.

The independent component that best overlaps the hand activation map is represented in figure 4.8. It is possible to recognize a strong activation in higher regions of the cortex, which disperse as the plane includes lower portions of the brain.

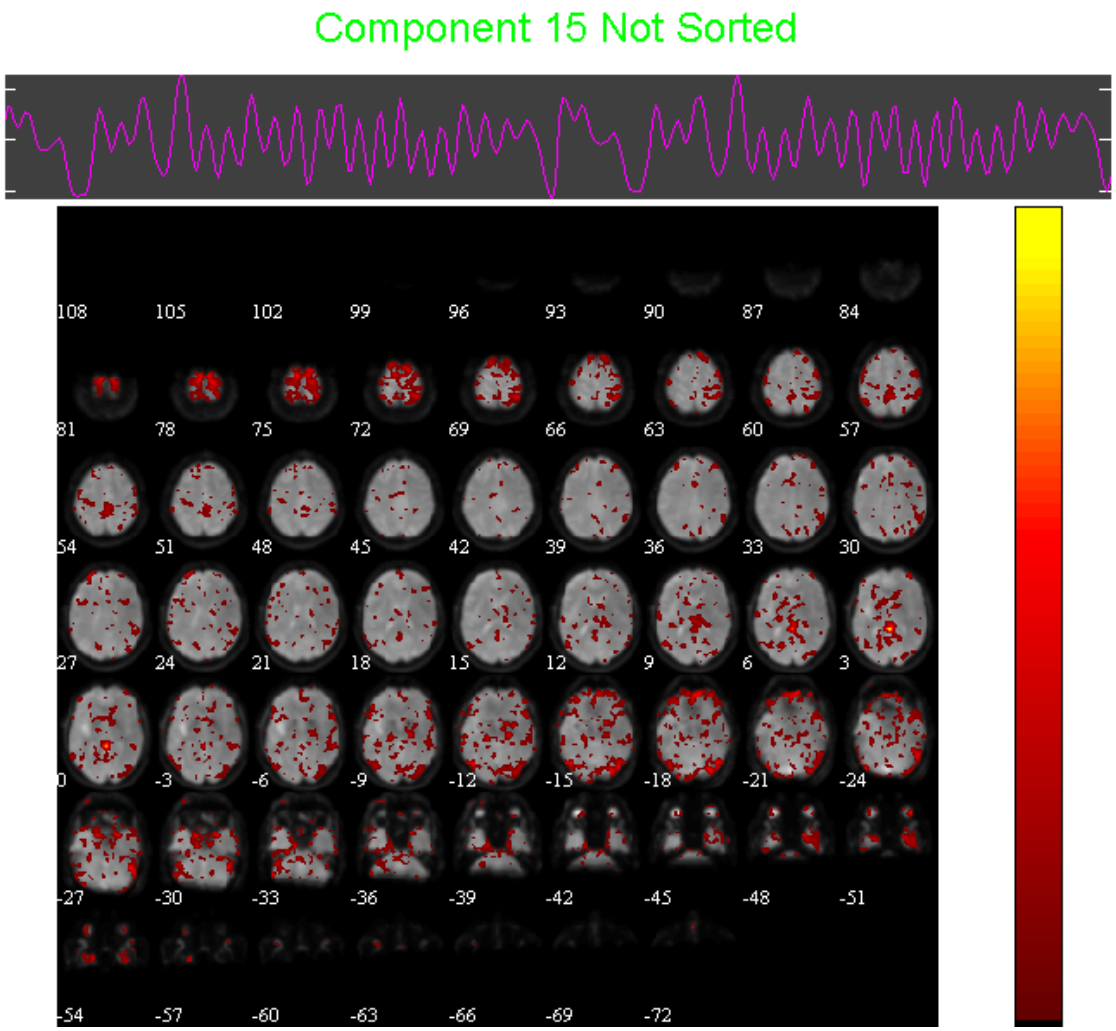

Figure 4.8: Independent Component of Sub003 rest network obtained in GIFT software. The figure consists of several transverse planes of the brain ordered from superior planes to inferiors.

The results of the similarity tests between resting-state and hands activation maps are displayed in table 4.2. The observed pattern repeats the tendency explained in the previous section, 4.2.1.1 .

Table 4.4: Similarity results for rest activation maps and hands paradigm activation maps for Sub003

	IC	Intensity Threshold	DSC (max)	IC	Intensity Threshold	SC1 (max)	IC	Intensity Threshold	SC2 (min)
FWE 0.01	41	0.1	0.0080	3	0.1	0.7143	41	0.1	0.9960
	15	0.1	0.0051	15	0.1	0.5714	15	0.1	0.9975
	15	0.2	0.0041	3	0.2	0.5476	15	0.2	0.9979
	10	0.1	0.0039	12	0.1	0.5476	10	0.1	0.9980
	41	0.2	0.0033	12	0.3	0.4762	41	0.2	0.9982
FWE 0.05	41	0.1	0.0103	3	0.1	0.6418	41	0.1	0.9948
	15	0.4	0.0076	15	0.1	0.5373	15	0.4	0.9949
	15	0.1	0.0076	3	0.2	0.4627	15	0.1	0.9962
	10	0.1	0.0059	12	0.1	0.4627	10	0.1	0.9970
	6	0.4	0.0055	41	0.1	0.3881	6	0.4	0.9972
FWE 0.1	41	0.1	0.0123	3	0.1	0.5333	41	0.1	0.9938
	15	0.1	0.0090	15	0.1	0.4778	15	0.4	0.9949
	6	0.4	0.0071	12	0.1	0.4556	15	0.1	0.9954
	15	0.2	0.0070	3	0.2	0.3778	15	0.2	0.9963
	15	0.4	0.0070	6	0.1	0.3778	6	0.1	0.9963
UNC 0.001	15	0.3	0.0459	15	0.1	0.3943	15	0.4	0.9541
	15	0.2	0.0430	23	0.1	0.3943	15	0.3	0.9617
	41	0.1	0.0333	6	0.1	0.3917	15	0.5	0.9661
	15	0.4	0.0311	12	0.1	0.3473	15	0.2	0.9742
	15	0.1	0.0308	3	0.1	0.3290	12	0.6	0.9746

4.2.1.3 Foot

The results of applying different statistical thresholds to the foot paradigm data is represented in the figure 4.9.

As in foot activation maps, for more restrictive *p*-values and its correction, the number of activations is smaller than in the case where no corrections were performed along with the statistical tests. Activation is located in the parasagittal precentral gyri in the two hemispheres, since the task is composed of the movement of both feet. There is also an isolated activation located between the Sylvian fissure and superior temporal sulcus.

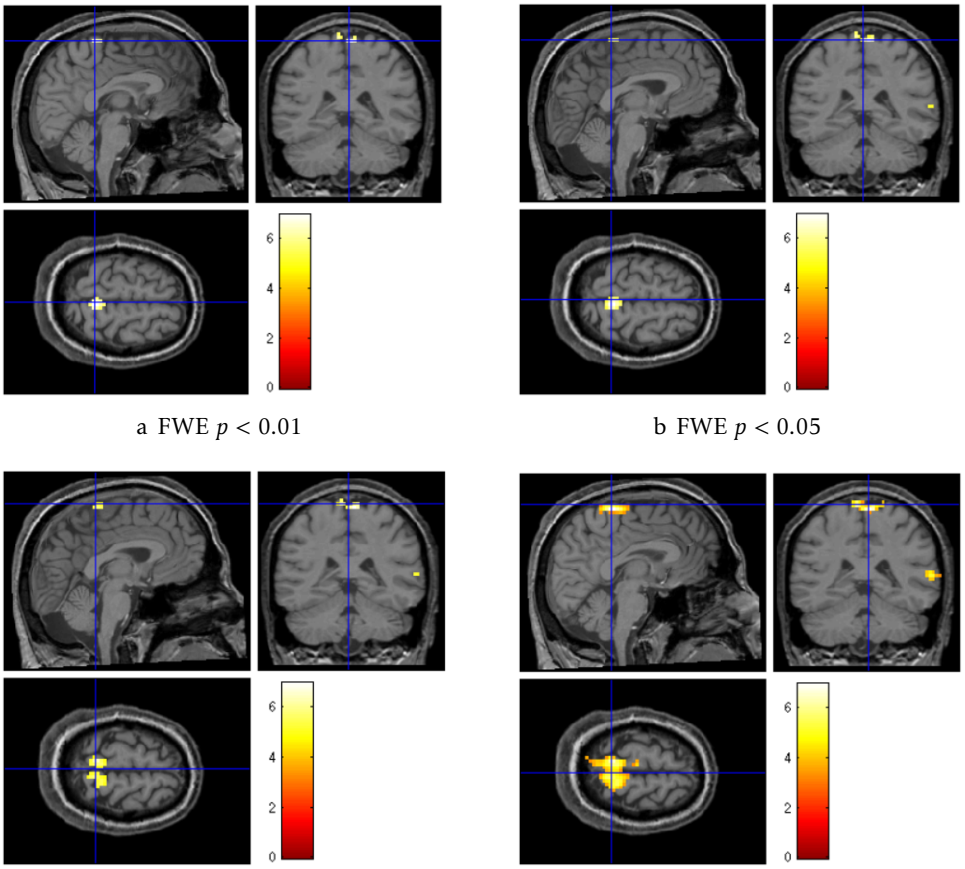

a FWE $p < 0.01$ b FWE $p < 0.05$

c FWE $p < 0.1$ d uncorrected $p < 0.001$

Figure 4.9: The 4 images at the top represent feet activation with distinct p-values a) p-value inferior to 0.01 FWE; b) p-value inferior to 0.05 FWE; c) p-value inferior to 0.1 FWE; d) p-value inferior to 0.001 uncorrected.

The independent component that best overlaps the foot activation map is represented in figure 4.10. It is possible to recognize a strong activation in higher regions of the cortex, upon the sagittal plane with high incidence in the posterior coronal planes. The activations disperse for medial transverse planes and once again have a high incidence in posterior regions for inferior transverse planes.

The results of the similarity tests between resting-state and foot activation maps are displayed in table 4.5. The results repeat the tendency observed in the similarity tests of mouth and hand paradigms and are explained in section 4.2.1.1

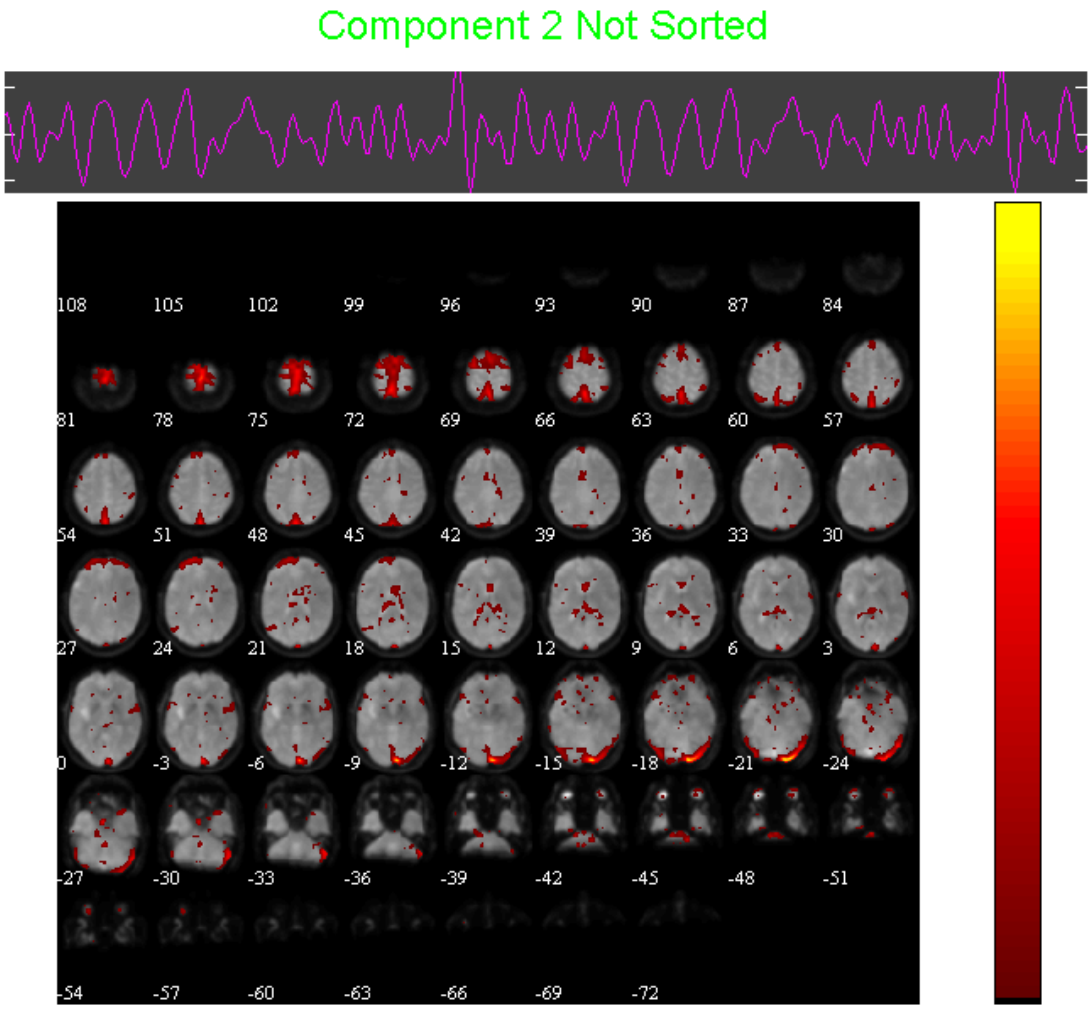

Figure 4.10: Independent Component of Sub003 rest network obtained in GIFT software. The figure consists of several transverse planes of the brain ordered from superior planes to inferiors.

Table 4.5: Similarity results for rest activation maps and feet paradigm activation maps for Sub003

	IC	Intensity Threshold	DSC (max)	IC	Intensity Threshold	SC1 (max)	IC	Intensity Threshold	SC2 (min)
FWE 0.01	2	0.2	0.0208	2	0.1	1	2	0.2	0.9895
	2	0.3	0.0118	6	0.1	0.9546	2	0.3	0.9940
	2	0.1	0.0109	7	0.1	0.8182	2	0.1	0.9945
	2	0.4	0.0089	2	0.2	0.7727	2	0.4	0.9953
	7	0.3	0.0086	6	0.2	0.7273	7	0.3	0.9956
FWE 0.05	2	0.2	0.0384	2	0.1	0.8600	2	0.2	0.9802
	2	0.3	0.0319	6	0.1	0.8600	2	0.3	0.9831
	2	0.4	0.0294	7	0.1	0.7200	2	0.4	0.9836
	2	0.5	0.0222	6	0.2	0.6600	2	0.5	0.9864
	2	0.1	0.0211	2	0.2	0.6400	2	0.1	0.9893
FWE 0.1	2	0.2	0.05	2	0.1	0.8594	2	0.2	0.9740
	2	0.3	0.0426	6	0.1	0.8594	2	0.4	0.9765
	2	0.4	0.0408	7	0.1	0.7031	2	0.3	0.9770
	2	0.1	0.0269	6	0.2	0.6719	2	0.1	0.9864
	7	0.3	0.0232	2	0.2	0.6563	2	0.5	0.9864
UNC 0.001	2	0.3	0.1079	6	0.1	0.5497	2	0.4	0.9249
	2	0.2	0.1053	2	0.1	0.4596	2	0.3	0.9250
	2	0.4	0.0856	49	0.1	0.4317	2	0.2	0.9369
	2	0.1	0.0680	7	0.1	0.3975	2	0.5	0.9409
	7	0.3	0.0505	6	0.2	0.3882	15	0.4	0.9592

4.2.1.4 Multi-motor task

Since there is no resting state network that resembles with only one motor tasks described above, a map resulting of overlapping mouth, hand and foot activated regions was created. The results of that test are displayed in table 4.6. The displayed pattern repeats the individual tendency of each task, which is, Dice Similarity Coefficient (DSC) has the lowest correlation values among the 3 similarity coefficients, whereas the Similarity Coefficient 2 has the highest outcomes. The similarity values of DSC increase for p-values less conservative, while SC_1 and SC_2values decrease.

The great difference that exists is the loss of sensitivity, i.e., the SC_1 is lower in the overlapping than in each task individually.

Table 4.6: Similarity test results for rest activation maps and with the result of the superposition of the 3 motor tasks for Sub003

	IC	Intensity Threshold	DSC (max)	IC	Intensity Threshold	SC1 (max)	IC	Intensity Threshold	SC2 (min)
FWE 0.01	2	0.2	0.0199	3	0.1	0.5368	2	0.2	0.9895
	2	0.3	0.0108	33	0.1	0.4737	2	0.3	0.9940
	2	0.1	0.0107	12	0.1	0.4211	2	0.1	0.9945
	15	0.2	0.0100	3	0.2	0.4105	15	0.2	0.9947
	41	0.1	0.0087	35	0.1	0.3895	2	0.4	0.9953
FWE 0.05	2	0.2	0.0356	3	0.1	0.4778	2	0.2	0.9802
	2	0.3	0.0278	33	0.1	0.4389	2	0.3	0.9831
	2	0.4	0.0231	35	0.1	0.4000	2	0.4	0.9836
	2	0.1	0.0204	6	0.1	0.3889	2	0.5	0.9864
	15	0.2	0.0183	3	0.2	0.3611	2	0.1	0.9893
FWE 0.1	2	0.2	0.0454	33	0.1	0.4249	2	0.2	0.9740
	2	0.3	0.0358	3	0.1	0.4163	2	0.4	0.9765
	2	0.4	0.0303	6	0.1	0.4034	2	0.3	0.9770
	2	0.1	0.0263	35	0.1	0.3863	2	0.1	0.9861
	15	0.2	0.0244	15	0.1	0.3476	15	0.2	0.9863
UNC 0.001	2	0.2	0.0859	33	0.1	0.3983	15	0.4	0.9184
	2	0.3	0.0719	6	0.1	0.3655	2	0.3	0.9190
	2	0.1	0.0703	3	0.1	0.3539	2	0.4	0.9249
	15	0.2	0.0675	35	0.1	0.3250	15	0.3	0.9252
	15	0.3	0.0533	50	0.1	0.2970	2	0.2	0.9295

4.2.2 Language

4.2.2.1 Semantic Decisions

The semantic decisions of this subject produced no significant activations, so the assessment of the similarity between task activated maps and rest maps is meaningless.

4.2.2.2 Syntactic Decisions

The results of applying different statistical thresholds to the syntactic paradigm data is represented in the figure 4.11.

For more restrictive p-values and its correction, the number of activated regions is smaller than in the case where no corrections were performed along with the statistical tests.

The activation produced by syntactical decision is robust. For lower axial planes, is evident a bilateral activation located in the middle temporal gyrus, illustrated in subfigures a, b, c (figure 4.11). For superior axial planes there is a great activation near the Broca's area in the right hemisphere and a small activation close to the Wernicke's area in the contralateral hemisphere. It is also important to mention that the cerebellum is another area with prominent activation.

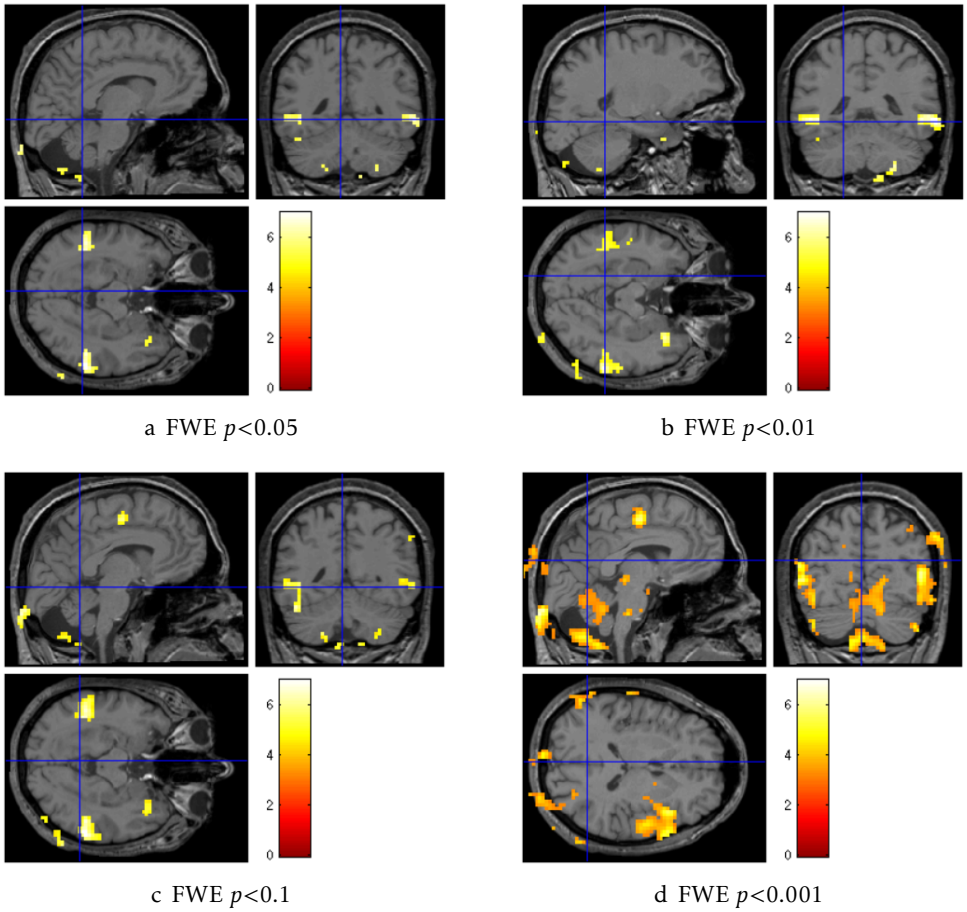

a FWE p<0.05

b FWE p<0.01

c FWE p<0.1

d FWE p<0.001

Figure 4.11: The 4 images at the top represent syntatic decisions activation with distinct p-values a) p-value inferior to 0.01 FWE; b) p-value inferior to 0.05 FWE; c) p-value inferior to 0.1 FWE; d) p-value inferior to 0.001 uncorrected.

The independent component that best overlaps the syntactic decision map is represented in figure 4.12. In the superior axial planes there is a strong activity in the anterior cortex area. As the planes are reaching the lower portions of the cortex, the activated regions become more dispersed with a clear dominance of the right hemisphere.

The results of the similarity tests between resting-state and syntactic decision activation maps are displayed in table 4.7. The results repeat the tendency observed in the similarity tests of motor paradigms and are explained in section 4.2.1.1

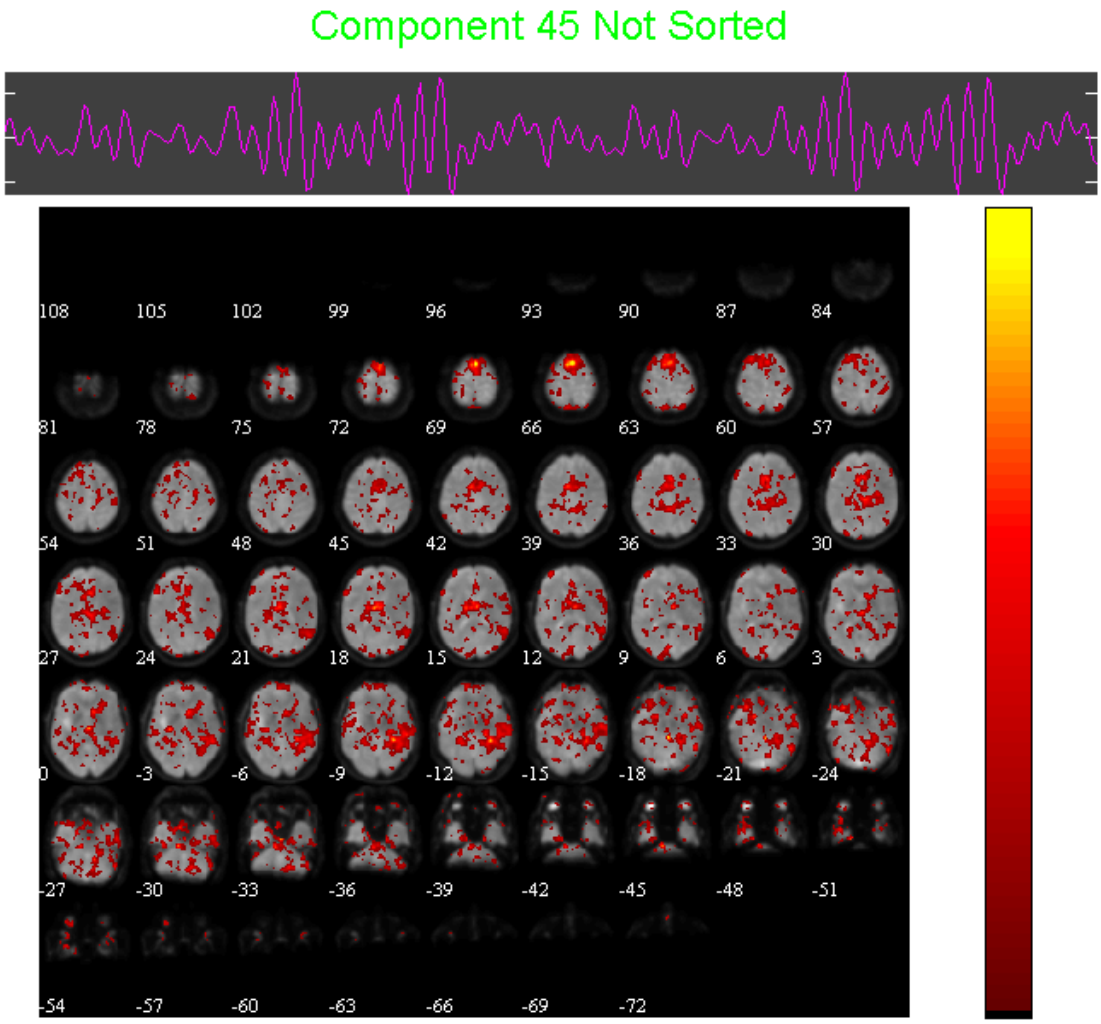

Figure 4.12: Independent Component of Sub003 rest network obtained in GIFT software. The figure consists of several transverse planes of the brain ordered from superior planes to inferiors.

Table 4.7: Similarity results for rest activation maps and syntactic decision paradigm activation maps for Sub003

	IC	Intensity Threshold	DSC (max)	IC	Intensity Threshold	SC1 (max)	IC	Intensity Threshold	SC2 (min)
FWE 0.01	6	0.7	0.0347	45	0.1	0.4847	6	0.8	0.8667
	6	0.8	0.0297	36	0.1	0.3593	6	0.7	0.9438
	6	0.6	0.0294	16	0.1	0.3566	6	0.6	0.9737
	45	0.2	0.0197	7	0.1	0.2813	26	0.5	0.9863
	45	0.3	0.0190	45	0.2	0.2786	6	0.5	0.9888
FWE 0.05	45	0.2	0.0360	45	0.1	0.4219	6	0.8	0.8000
	45	0.3	0.0348	36	0.1	0.3326	6	0.7	0.9250
	39	0.1	0.0287	16	0.1	0.3187	26	0.5	0.9589
	45	0.1	0.0282	45	0.2	0.2452	26	0.6	0.9615
	16	0.2	0.0280	35	0.1	0.2323	6	0.6	0.9650
FWE 0.1	45	0.2	0.0439	45	0.1	0.3998	6	0.8	0.800
	45	0.3	0.0410	16	0.1	0.3057	6	0.7	0.9250
	16	0.3	0.0384	36	0.1	0.2917	6	0.6	0.9584
	16	0.2	0.0368	35	0.1	0.2283	26	0.5	0.9584
	45	0.1	0.0365	45	0.2	0.2218	26	0.6	0.9615
UNC 0.001	45	0.1	0.1327	45	0.1	0.3216	23	0.9	0.5000
	45	0.2	0.1219	36	0.1	0.2693	26	0.8	0.5000
	16	0.1	0.1199	16	0.1	0.2595	26	0.9	0.5000
	19	0.1	0.1179	23	0.1	0.2595	27	0.9	0.5000
	36	0.1	0.1170	3	0.1	0.2586	23	0.8	0.5676

4.2.2.3 Verb Generation

The results of applying different statistical thresholds to the verb generation data is represented in the figure 4.13.

From the image is possible to find a robust activation upon sagittal plane immediately above the corpus callosum. For less restrictive p-values, the superior temporal gyrus appears activated immediately beneath the Sylvian fissure in both hemispheres.

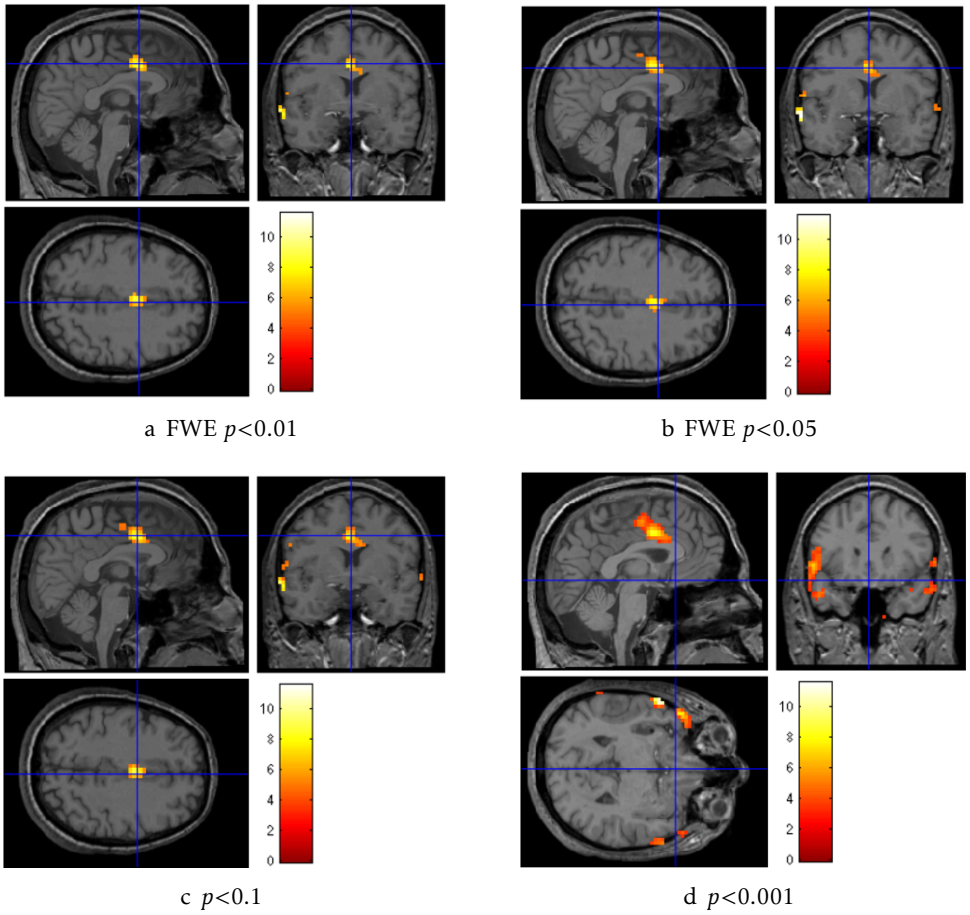

a FWE p<0.01 b FWE p<0.05

c p<0.1 d p<0.001

Figure 4.13: Independent Component of Sub003 rest network obtained in GIFT software. The figure consists of several transverse planes of the brain ordered from superior planes to inferiors.

The independent component that best overlaps the verb generation map is represented in figure 4.14. It is possible to verify a large laterality of activations for the left hemisphere along all planes.

The results of the similarity tests between resting-state and verb generation activation maps are displayed in table 4.8. The results repeat the tendency observed in the similarity tests of motor paradigms and are explained in section 4.2.1.1

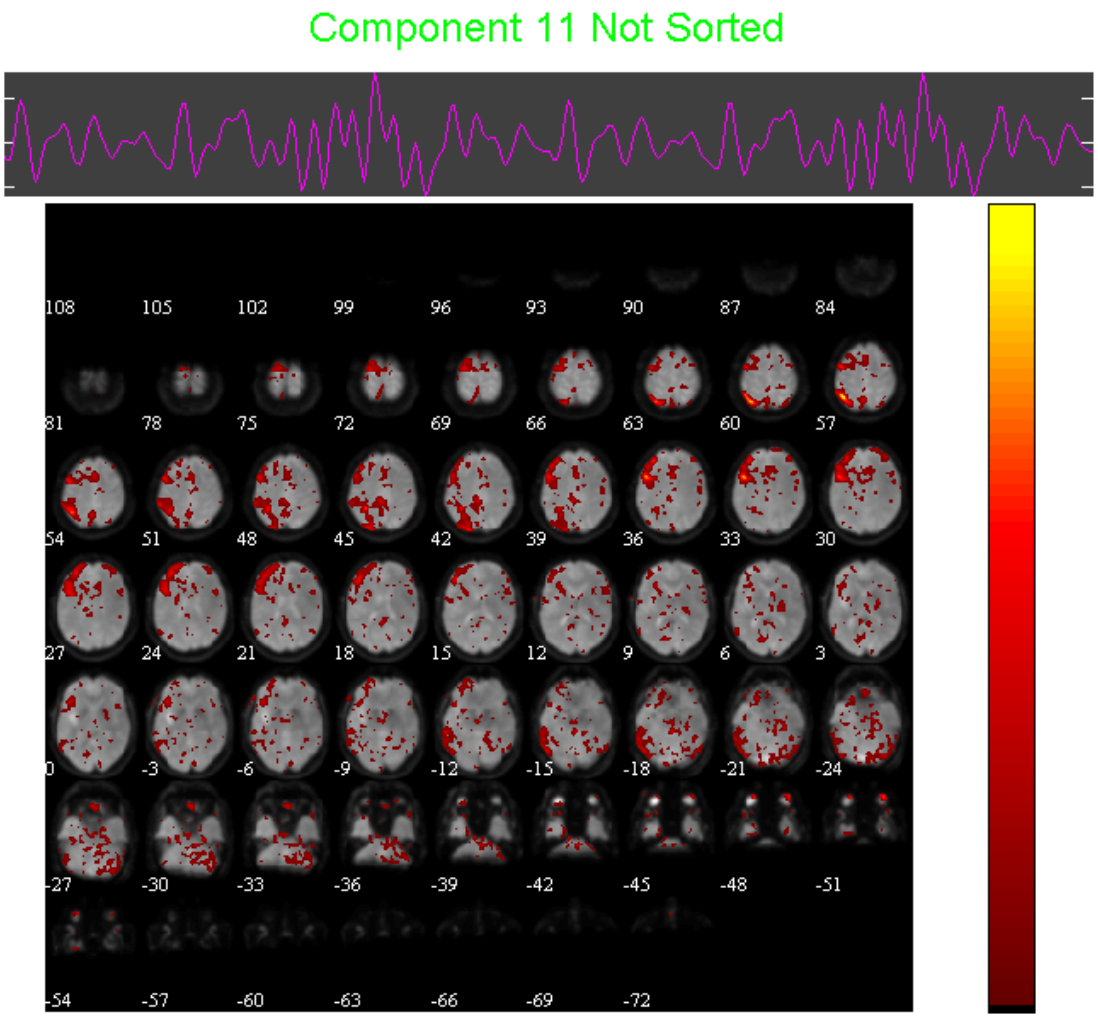

Figure 4.14: Independent Component of Sub003 rest network obtained in GIFT software. The figure consists of several transverse planes of the brain ordered from superior planes to inferiors.

Table 4.8: Similarity test results for rest activation maps and verb generation paradigm activation maps for Sub003

	IC	Intensity Threshold	DSC (max)	IC	Intensity Threshold	SC1 (max)	IC	Intensity Threshold	SC2 (min)
FWE 0.01	11	0.3	0.0451	11	0.1	0.5787	11	0.3	0.9720
	11	0.2	0.0451	6	0.1	0.4676	11	0.2	0.9754
	11	0.4	0.0340	45	0.1	0.4074	6	0.8	0.9778
	11	0.1	0.0253	33	0.1	0.3796	11	0.4	0.9732
	33	0.3	0.0226	35	0.1	0.3796	11	0.5	0.9803
FWE 0.05	11	0.2	0.0658	11	0.1	0.5247	6	0.8	0.9333
	11	0.3	0.0573	6	0.1	0.4231	11	0.3	0.9597
	11	0.4	0.0407	45	0.1	0.4121	11	0.4	0.9598
	11	0.1	0.0380	33	0.1	0.3709	11	0.2	0.9621
	8	0.2	0.0357	16	0.1	0.3681	11	0.5	0.9137
FWE 0.1	11	0.2	0.0747	11	0.1	0.5126	6	0.8	0.9111
	11	0.3	0.0663	6	0.1	0.4345	11	0.3	0.9507
	11	0.1	0.0441	45	0.1	0.4207	11	0.4	0.9544
	8	0.2	0.0423	35	0.1	0.3701	11	0.2	0.9559
	11	0.4	0.0421	16	0.1	0.3655	11	0.5	0.9671
UNC 0.001	11	0.2	0.1359	11	0.1	0.4086	6	0.8	0.6667
	11	0.1	0.1086	45	0.1	0.3837	6	0.9	0.7143
	11	0.3	0.0909	6	0.1	0.3830	6	0.7	0.8500
	39	0.1	0.0768	35	0.1	0.3439	11	0.4	0.8740
	8	0.2	0.0720	16	0.1	0.3419	11	0.3	0.8791

4.2.2.4 Multi-language task

Similarly to motor tasks, an overlay map of the three linguistic tasks was created and compared with the resting state map. The results of that test are displayed in table 4.9. The displayed pattern repeats the individual tendency of each task, which is, Dice Similarity Coefficient (DSC) has the lowest correlation values among the 3 similarity coefficients, whereas the Similarity Coefficient 2 has the highest outcomes. The similarity values of DSC increase for p-values less conservative, while SC_1 and SC_2values decrease.

Table 4.9: Similarity test results for rest activation maps and with the result of the superposition of the 3 motor tasks for Sub003

	IC	Intensity Threshold	DSC (max)	IC	Intensity Threshold	SC1 (max)	IC	Intensity Threshold	SC2 (min)
FWE 0.01	11	0.2	0.0405	45	0.1	0.4520	6	0.8	0.8667
	11	0.3	0.0344	16	0.1	0.3594	6	0.7	0.9438
	11	0.1	0.0301	36	0.1	0.3025	11	0.3	0.9720
	39	0.1	0.0298	35	0.1	0.2900	11	0.4	0.9732
	45	0.2	0.0263	6	0.1	0.2829	6	0.6	0.9737
FWE 0.05	11	0.2	0.0542	45	0.1	0.4114	8	0.9	0.0000
	39	0.1	0.0459	16	0.1	0.3351	8	0.8	0.6667
	45	0.2	0.0456	36	0.1	0.2870	8	0.7	0.7273
	11	0.1	0.0453	35	0.1	0.2752	6	0.8	0.8000
	45	0.3	0.0419	6	0.1	0.2407	8	0.6	0.9000
FWE 0.1	11	0.2	0.0574	45	0.1	0.4008	8	0.9	0.0000
	45	0.2	0.0554	16	0.1	0.3194	8	0.7	0.5455
	11	0.1	0.0546	36	0.1	0.2695	8	0.8	0.6667
	39	0.1	0.0519	35	0.1	0.2688	8	0.6	0.8000
	45	0.3	0.0508	6	0.1	0.2421	6	0.8	0.8000
UNC 0.001	45	0.1	0.1552	45	0.1	0.3275	8	0.8	0.0000
	16	0.1	0.1408	16	0.1	0.2756	8	0.9	0.0000
	45	0.2	0.1360	35	0.1	0.2695	8	0.7	0.0909
	37	0.1	0.1328	36	0.1	0.2639	8	0.6	0.4000
	11	0.1	0.1325	3	0.1	0.2620	26	0.9	0.5000

4.3 Intra-Task Analysis

This section aims to present the results in an intra-task perspective. Thus, the results of activations mapping of one task and at rest will be presented for all participants. The choice of the task, as mentioned earlier in this chapter, is related to the small number of volumes removed by scrubbing (consult table 4.1), and taking this into account the hand task was the selected paradigm.

- **Subject 001**

Table 4.10: Similarity test results for rest activation maps and hand activation maps for Sub001

	IC	Intensity Threshold	DSC (max)	IC	Intensity Threshold	SC1 (max)	IC	Intensity Threshold	SC2 (min)
FWE 0.01	45	0.2	0.2279	45	0.1	0.6941	45	0.9	0.6667
	45	0.3	0.1720	48	0.1	0.3706	45	0.5	0.6667
	45	0.1	0.1201	45	0.3	0.3000	45	0.4	0.6806
	45	0.4	0.1117	8	0.1	0.2412	45	0.6	0.6923
	45	0.5	0.0733	20	0.1	0.2118	45	0.7	0.7143
FWE 0.05	45	0.2	0.2411	45	0.1	0.6583	45	0.9	0.0000
	45	0.3	0.1659	48	0.1	0.3146	45	0.8	0.2500
	45	0.1	0.1651	45	0.2	0.2505	45	0.7	0.2857
	45	0.4	0.1056	20	0.1	0.2214	45	0.6	0.4615
	45	0.6	0.0718	8	0.1	0.2117	45	0.5	0.5238
FWE 0.1	45	0.2	0.2463	45	0.1	0.6421	45	0.9	0.0000
	45	0.1	0.1833	48	0.1	0.3010	45	0.8	0.2500
	45	0.3	0.1636	45	0.2	0.2375	45	0.7	0.2857
	45	0.4	0.1045	20	0.1	0.2191	45	0.6	0.3846
	45	0.5	0.0719	8	0.1	0.2157	45	0.5	0.4524
UNC 0.001	45	0.1	0.3035	45	0.1	0.4166	45	0.9	0.0000
	45	0.2	0.1975	20	0.1	0.2509	45	0.6	0.2308
	45	0.3	0.0920	8	0.1	0.2363	45	0.4	0.2361
	48	0.1	0.0856	48	0.1	0.2032	45	0.5	0.2381
	44	0.1	0.0718	21	0.1	0.1813	45	0.8	0.2500

- **Subject 002**

Table 4.11: Similarity test results for rest activation maps and hand activation maps for Sub002

	IC	Intensity Threshold	DSC (max)	IC	Intensity Threshold	SC1 (max)	IC	Intensity Threshold	SC2 (min)
FWE 0.01	36	0.3	0.0788	36	0.1	0.5174	36	0.4	0.9350
	36	0.2	0.0771	24	0.1	0.4636	36	0.5	0.9415
	24	0.3	0.0766	28	0.1	0.3759	24	0.5	0.9416
	24	0.2	0.0709	36	0.2	0.3062	24	0.6	0.9453
	36	0.4	0.0636	8	0.1	0.2735	36	0.3	0.9454
FWE 0.05	36	0.2	0.0843	36	0.1	0.4815	36	0.4	0.9294
	4	0.3	0.0815	24	0.1	0.4435	36	0.5	0.9328
	36	0.3	0.0786	28	0.1	0.3796	24	0.5	0.9380
	24	0.2	0.0776	36	0.1	0.2813	24	0.4	0.9393
	36	0.4	0.0620	8	0.1	0.2666	24	0.3	0.9397
FWE 0.1	36	0.2	0.0878	36	0.1	0.4742	36	0.4	0.9272
	24	0.3	0.0858	24	0.1	0.4409	36	0.5	0.9328
	24	0.2	0.0830	28	0.1	0.3862	24	0.4	0.9329
	36	0.3	0.0807	36	0.2	0.2728	24	0.5	0.9343
	36	0.4	0.0640	8	0.1	0.2601	24	0.3	0.9348
UNC 0.001	24	0.2	0.1283	24	0.1	0.3768	36	0.9	0.6667
	36	0.2	0.1153	36	0.1	0.3594	36	0.8	0.7368
	24	0.1	0.1142	28	0.1	0.3440	36	0.6	0.7823
	24	0.3	0.1082	8	0.1	0.2315	36	0.5	0.8333
	36	0.1	0.1054	24	0.2	0.1951	36	0.7	0.84314

- **Subject 003**

Table 4.12: Similarity test results for rest activation maps and hand activation maps for Sub003

	IC	Intensity Threshold	DSC (max)	IC	Intensity Threshold	SC1 (max)	IC	Intensity Threshold	SC2 (min)
FWE 0.01	41	0.1	0.0080	3	0.1	0.7143	41	0.1	0.9960
	15	0.1	0.0051	15	0.1	0.5714	15	0.1	0.9975
	15	0.2	0.0041	3	0.2	0.5476	15	0.2	0.9979
	10	0.1	0.0040	12	0.1	0.5476	10	0.1	0.998
	1	0.2	0.0033	12	0.3	0.4762	41	0.2	0.9982
FWE 0.05	41	0.1	0.0103	3	0.1	0.6418	41	0.1	0.9948
	15	0.4	0.0076	15	0.1	0.5373	15	0.4	0.9950
	15	0.1	0.0076	3	0.2	0.4627	15	0.1	0.9962
	10	0.1	0.0059	12	0.1	0.4627	10	0.1	0.9970
	6	0.4	0.055	41	0.1	0.3881	6	0.4	0.9972
FWE 0.1	41	0.1	0.0123	3	0.1	0.5333	41	0.1	0.9938
	15	0.1	0.0090	15	0.1	0.4778	15	0.4	0.9949
	6	0.4	0.0071	12	0.1	0.4556	15	0.1	0.9954
	15	0.2	0.0070	3	0.2	0.3778	15	0.2	0.9963
	15	0.4	0.0070	6	0.1	0.3778	6	0.1	0.9963
UNC 0.001	15	0.3	0.0459	15	0.1	0.3943	15	0.4	0.9541
	15	0.2	0.0430	23	0.1	0.3943	15	0.3	0.9617
	41	0.1	0.0333	6	0.1	0.3961	15	0.5	0.9661
	15	0.4	0.0311	12	0.1	0.3473	15	0.2	0.9742
	15	0.1	0.0308	3	0.1	0.3290	12	0.6	0.9746

- **Subject 004**

Table 4.13: Similarity test results for rest activation maps and hand activation maps for Sub004

	IC	Intensity Threshold	DSC (max)	IC	Intensity Threshold	SC1 (max)	IC	Intensity Threshold	SC2 (max)
FWE 0.01	46	0.1	0.0370	2	0.1	0.2712	46	0.1	0.9797
	27	0.1	0.0340	50	0.1	0.2522	50	0.3	0.9805
	50	0.2	0.0311	40	0.1	0.2366	50	0.4	0.9811
	15	0.1	0.0305	46	0.1	0.2106	27	0.1	0.9813
	50	0.1	0.0297	27	0.1	0.1932	50	0.2	0.9819
FWE 0.05	46	0.1	0.0426	50	0.1	0.2732	50	0.4	0.9689
	50	0.2	0.0426	2	0.1	0.2496	50	0.5	0.9695
	27	0.1	0.0406	40	0.1	0.2382	50	0.3	0.9700
	50	0.3	0.0403	46	0.1	0.2039	50	0.2	0.9746
	50	0.1	0.0385	44	0.1	0.1946	50	0.6	0.9748
FWE 0.1	50	0.2	0.0487	50	0.1	0.2846	50	0.4	0.9639
	46	0.1	0.0479	40	0.1	0.2421	50	0.5	0.9659
	50	0.1	0.0441	2	0.1	0.2389	50	0.6	0.9664
	50	0.3	0.0430	46	0.1	0.2086	50	0.3	0.9669
	27	0.1	0.0428	44	0.1	0.2022	40	0.5	0.9674
UNC 0.001	50	0.2	0.0939	50	0.1	0.3121	50	0.5	0.9066
	50	0.1	0.0920	40	0.1	0.2303	50	0.4	0.9115
	46	0.1	0.0825	44	0.1	0.2122	50	0.6	0.9118
	50	0.3	0.0739	46	0.1	0.1962	50	0.3	0.9220
	44	0.1	0.0682	2	0.1	0.1811	40	0.6	0.9316

- **Subject 005**

Table 4.14: Similarity test results for rest activation maps and hand activation maps for Sub005

	IC	Intensity Threshold	DSC (max)	IC	Intensity Threshold	SC1 (max)	IC	Intensity Threshold	SC2 (min)
FWE 0.01	46	0.4	0.0603	8	0.1	0.5388	46	0.7	0.8974
	46	0.5	0.0541	7	0.1	0.4306	46	0.6	0.9240
	46	0.3	0.0506	8	0.2	0.3765	46	0.5	0.9403
	31	0.1	0.0461	12	0.1	0.3718	46	0.4	0.9490
	46	0.6	0.0436	7	0.2	0.3271	46	0.8	0.9615
FWE 0.05	46	0.4	0.0692	8	0.1	0.5248	46	0.7	0.8590
	46	0.3	0.0617	7	0.1	0.4046	46	0.6	0.9006
	46	0.5	0.0571	8	0.2	0.3664	46	0.8	0.9231
	31	0.1	0.0517	12	0.1	0.3416	46	0.5	0.9290
	46	0.6	0.0489	7	0.2	0.2996	46	0.4	0.9353
FWE 0.1	46	0.4	0.0692	8	0.1	0.4983	46	0.7	0.8590
	46	0.3	0.0619	7	0.1	0.4072	46	0.6	0.9006
	46	0.5	0.0557	8	0.2	0.3471	46	0.8	0.9231
	31	0.1	0.0547	12	0.1	0.3368	46	0.5	0.9261
	8	0.2	0.0459	7	0.2	0.2921	46	0.4	0.9320
UNC 0.001	46	0.3	0.0885	8	0.1	0.2946	31	0.9	0.6000
	46	0.2	0.0869	7	0.1	0.2550	46	0.7	0.6667
	31	0.1	0.0831	12	0.1	0.2363	46	0.8	0.6923
	46	0.4	0.0819	45	0.1	0.2062	46	0.6	0.7368
	45	0.1	0.0690	46	0.1	0.2006	46	0.5	0.8040

- **Subject 006**

Table 4.15: Similarity test results for rest activation maps and hand activation maps for Sub006

	IC	Intensity Threshold	DSC (max)	IC	Intensity Threshold	SC1 (max)	IC	Intensity Threshold	SC2 (max)
FWE 0.01	44	0.1	0.0076	6	0.1	0.3684	14	0.5	0.9954
	40	0.3	0.0071	44	0.1	0.3211	44	0.1	0.9962
	40	0.2	0.0069	40	0.1	0.2737	40	0.3	0.9962
	40	0.1	0.0059	6	0.2	0.2105	40	0.2	0.9965
	14	0.5	0.0049	30	0.1	0.2053	40	0.1	0.9970
FWE 0.05	44	0.1	0.0117	6	0.1	0.3709	44	0.1	0.9940
	40	0.1	0.0095	44	0.1	0.3146	14	0.4	0.9948
	40	0.2	0.0091	40	0.1	0.2781	40	0.1	0.9952
	30	0.1	0.0078	30	0.1	0.2351	40	0.2	0.9953
	40	0.3	0.0075	6	0.1	0.2318	14	0.5	0.9954
FWE 0.1	44	0.1	0.0138	6	0.1	0.3714	14	0.4	0.9922
	40	0.1	0.0111	44	0.1	0.3200	44	0.1	0.9930
	40	0.2	0.0108	40	0.1	0.2829	44	0.4	0.9934
	40	0.3	0.0092	6	0.2	0.2257	14	0.3	0.9937
	14	0.3	0.0087	30	0.1	0.2171	40	0.1	0.9943
UNC 0.001	40	0.3	0.0426	6	0.1	0.3529	41	0.8	0.8889
	40	0.2	0.0426	40	0.1	0.3417	41	0.6	0.8889
	40	0.1	0.0397	44	0.1	0.2998	43	0.7	0.9091
	44	0.1	0.0379	6	0.2	0.2142	41	0.7	0.9130
	40	0.4	0.0317	30	0.1	0.1993	5	0.6	0.9167

- **Subject 007**

Table 4.16: Similarity test results for rest activation maps and hand activation maps for Sub007

	IC	Intensity Threshold	DSC (max)	IC	Intensity Threshold	SC1 (max)	IC	Intensity Threshold	SC2 (min)
FWE 0.01	20	0.2	0.0336	24	0.1	0.2782	20	0.4	0.9461
	20	0.3	0.0297	34	0.1	0.2770	20	0.3	0.9651
	34	0.1	0.0246	32	0.1	0.2688	39	0.4	0.9778
	39	0.3	0.0231	39	0.1	0.2453	20	0.2	0.9780
	34	0.2	0.0218	20	0.1	0.1690	39	0.3	0.9841
FWE 0.05	20	0.2	0.0417	34	0.1	0.2834	20	0.4	0.9401
	34	0.1	0.0325	24	0.1	0.2816	20	0.3	0.9556
	20	0.3	0.0321	32	0.1	0.2726	20	0.2	0.9706
	39	0.3	0.0296	39	0.1	0.2610	39	0.4	0.9753
	34	0.2	0.024	20	0.1	0.1785	39	0.3	0.9779
FWE 0.1	20	0.2	0.0475	34	0.1	0.2842	20	0.4	0.9281
	20	0.3	0.0377	24	0.1	0.2795	20	0.3	0.9429
	34	0.1	0.0371	39	0.1	0.2787	20	0.2	0.9651
	34	0.2	0.0339	32	0.1	0.2732	39	0.4	0.9741
	39	0.1	0.0337	20	0.1	0.1842	39	0.3	0.9744
UNC 0.001	39	0.1	0.1022	39	0.1	0.3259	15	0.9	0.5000
	20	0.1	0.1019	24	0.1	0.3005	12	0.8	0.6364
	39	0.2	0.0891	32	0.1	0.2562	15	0.8	0.6875
	12	0.1	0.0836	12	0.1	0.2491	24	0.9	0.7143
	20	0.2	0.0826	20	0.1	0.2367	12	0.7	0.8182

- **Subject 008**

Table 4.17: Similarity test results for rest activation maps and hand activation maps for Sub008

	IC	Intensity Threshold	DSC (max)	IC	Intensity Threshold	SC1 (max)	IC	Intensity Threshold	SC2 (min)
FWE 0.01	19	0.1	0.1204	19	0.1	0.4092	19	0.9	0.0000
	19	0.2	0.1151	31	0.1	0.3598	19	0.8	0.4444
	19	0.3	0.1053	2	0.1	0.3233	19	0.7	0.6552
	19	0.4	0.0773	9	0.1	0.2412	19	0.6	0.6932
	9	0.1	0.0732	45	0.1	0.1850	19	0.5	0.7317
FWE 0.05	19	0.1	0.1633	19	0.1	0.4021	19	0.9	0.0000
	19	0.2	0.1445	31	0.1	0.3306	19	0.8	0.4444
	19	0.3	0.1176	2	0.1	0.2935	19	0.7	0.5172
	9	0.1	0.1000	9	0.1	0.2393	19	0.6	0.6023
	9	0.2	0.0929	45	0.1	0.1855	19	0.5	0.6146
FWE 0.1	19	0.1	0.1840	19	0.1	0.3934	19	0.9	0.0000
	19	0.2	0.1545	31	0.1	0.3215	19	0.8	0.1111
	19	0.3	0.1197	2	0.1	0.2835	19	0.7	0.3793
	9	0.1	0.1141	9	0.1	0.2373	19	0.6	0.5114
	31	0.1	0.1010	21	0.1	0.1924	19	0.5	0.5561
UNC 0.001	19	0.1	0.3220	19	0.1	0.3097	19	0.9	0.0000
	31	0.1	0.2348	31	0.1	0.2949	19	0.7	0.0690
	9	0.1	0.2310	2	0.1	0.2355	19	0.8	0.1111
	6	0.1	0.2146	6	0.1	0.2311	10	0.7	0.1304
	45	0.1	0.2097	9	0.1	0.2184	19	0.6	0.1364

The task under analysis has a low similarity to rest data of the respective subject.

The maximum DSC was approximately 30.35% for the subject001 and the maximum value of SC_1 was 71.43% for the subject 003.The subject with the most satisfactory coefficients is the Sub008, with DSC = 12%, SC_1 = 40.92%, and finally a SC_2 = 0%. On the other hand, the subject with less satisfactory coefficients was the subject 006 with DSC = 0.76%, SC1= 36.84% and SC2 = 99.54%.

4.4 Results Overview

Given the large volume of results, and the consequent impossibility of presenting all of them, this section aims to provide an overview of the results.

In general the results follow tendency observed in the examples described above in this section. The values of Dice similarity coefficient are those with the greatest variations among tasks and subjects, but are in all cases low and always lower than the Similarity Coefficient 1 and Similarity Coefficient 2. In the case of SC_1, the values obtained were reasonable in most cases while SC_2 values were generally close to 1. The similarity values of DSC increase for p-values less conservative, while SC_1 and SC_2values generally decrease. The increase in DSC values means that the performance of too restrictive statistical thresholds leads to the removal of activated task regions that are coincident with the activated regions in resting state. The decline in the latter coefficients derives from the increased activated mouth regions as result of application of a low restrictive statistical threshold.

From the perspective of tasks, semantic decision was the one that had worse results and in many cases there were no overlaps between the task data and rest, resulting in a DSC ans SC_1 equals to 0 and SC_2 equals to 1. Excluding these cases, the syntactic decision showed the lowest values in SC_1. In parallel, the verbal generation was the task that presented higher SC_1 values. With regard to SC_2, it did not presented a pattern among tasks, where in the range of values showed no relation to the task nature.

Chapter 5

Discussion

The task-free nature of rs-fMRI has propelled many studies of brain connectivity. Efforts are being made to translate these studies into clinical practice. In this study, we explored the feasibility of resting-state fMRI as a complement to task-based fMRI for presurgical planning.

In order to accomplish the goal of this study, we first explored all preprocessing parameters and conceived the most efficient protocol.

To correct the effects of head movement in the BOLD signal in task-based fMRI we refer to scrubbing and 6 realignment parameters regression. We noticed a greater impact of scrubbing on linguistic tasks. The origin of this trend may be related to two factors coming from the architecture of these paradigms. The first is the high frequency of the stimulus occurrence, and the second is the response requirements. The demand for a quick response can lead to unintentional micro-movements. Semantic decision was the task that had a higher number of scrubbed volumes, and hence the one that involved a greater head movement. Among motor tasks, feet movement was the one that induced the greatest amount of volumes scrubbed, followed by mouth and hand movement. In the first case the translation in the z-axis and rotation in the y-axis implied by foot motion induces movement over the whole body, thereby causing head displacements. As regards to the mouth task, it entails the movement of the jaw causing undesired head movements. Finally, hand paradigms was the task that causes less displacements because of the limited motor exigency of the task.

In resting-state fMRI we established two approaches, the first was to repeat the procedure used in task and the second was to additionally remove intrinsic signals to the brain - nuisance covariates removal. We followed the protocol used by Yan et al. (2013) [55], which regressed out WM and CSF, however adding further global signal regressor, an approach taken by Satterthwaite et al. (2013) [57]. However, countering to these studies, we realized that this latter led to results that were visually worse and had a more pronounced effect in the extraction of independent components, resulting in poorer outcomes in the analysis of similarity with task data. The source of these worse results can arise from the processing protocol chosen by us. A possible reintroduction of artefacts into the RS-fcMRI time series could be avoided by the simultaneous performance of nuisance signals regression and filtering, as proposed by Hallquist et al. (2013) [58]. Notwithstanding, the performance of any two processes simultaneously was unattainable due to the particularities of the used software (DPARSFA).

In this study we have also found a strong relationship between the age of participants and the number of volumes removed by scrubbing. In our sample, the younger subjects were those who performed the largest number of displacements per task. These results are consistent with previous studies (Power et al.(2012), Satterthwaite et al., (2012) and Yan et al. [56] [57] [55]). The study carried out by Power demonstrated how scrubbing may change fundamental conclusions about patterns of functional connectivity. This can be particularly critical in rest data, since the efficiency of resting-state networks extraction is result of a good separation of independent components. In our study, a large decrease of volumes has not meant a visually different spatial distribution of the regions activated. Although, the application of a less strict framewise displacement threshold, such as FD > 0.7 mm, could improve the similarity analysis results.

Another preprocessing step that can be the source of introducing artifacts is normalization. Brain normalization is important for individual subjects, and not only for inter-subject data, since it allows to establish relations between regions activated from the rest and task maps maps when the fields of view of rest and task acquisitions do not match. Despite the need of its application, there is no guarantee that there were no misaligned structures between different paradigms, which consequently may result in false negative and positive activations.

As regards to task data processing, most of the results are visually concordant with the expectations from the literature and clinical practice. A subset of the data was assessed by an experienced neurologist who confirmed the consistency of the results.

However, the observed variations may be due not only to the spikes in BOLD signal from the micro-movements of the head, but also to a natural adjustment of the brain. The plasticity of the brain is an important variable to take into account in the study of functional and resting state networks, especially in pre-surgical planning. In these cases, it is especially crucial to choose a good set of statistical thresholds. In this study we explore the influence of the application of 4 distinct *p*-values (0.01 FWE; 0.05 FWE; 0.1 FWE and 0.001 UNC). For more stringent thresholds, important activated regions were no longer visible, or the extent of activation was not fully covered. In contrast, when *p*-values were more lenient, false positive activations emerged. It is therefore impossible to draw any conclusion about what the best threshold is.Rather, information stemming from several , p-values should be taken into consideration during the process and will result in an informed analysis about the location and extent of the areas to be avoided in surgical resection. This assumption has a direct impact on the calculation of the similarity between the task and rest data. Low statistical thresholds authenticate the specificity of the overlap, yet imply low sensitivity. On the other hand, sensitivity increases for higher *p*-values, thereby not guaranteeing specific results.

To process the resting-state data, our approach was to replicate the procedures performed in several previous studies involving the same software (GIFT). Therefore, we generated ICA maps for 20 and 50 independent components, following a rough approach of Sair et al. (2015) [42]. As they reported, the similarity analysis improved with increasing the number of extracted components. Accordingly, we performed independent component analysis resorting to 50 IC in order to obtain the best concordance with task maps. Even so, there was no evident observable similarity between the independent components extracted for each participant with the well-known default mode networks. Despite the impossibility of choosing an ideal number of independent components highlighted by Hui et al. (2011), the number of components to be extracted is crucial, since for a low number of IC, different brain networks may merge, while for higher numbers there is a risk of splitting a relevant network into several ICs. Another reason for the discrepancy between the areas activated at rest and the expected default mode networks can result from the choice of the algorithm that tests the stability and reliability of independent components, such as its amount of runs. Because of the scarce information found in the literature, the chosen algorithm was the one that was used in similar studies (ICASSO). As regards to the number of times that the algorithm runs, we opted for a relatively low number (compared with the number mentioned in Tie et al.(2014) [44]) because of the high computation time that the procedure requires. The application of another algorithm and a greater number of runs could potentially lead

to extracting resting state networks more resembling to task networks.

Finally, we performed three analysis of similarity between the rest maps and the map of each of the six tasks for every subject.

The first coefficient, Dice Similarity Coefficient, was previously used in several other studies, including Sair et al. (2015) [42] and Branco et al. (2016) [43]. In the scope of this study, this index can be referred as an appraiser of the specificity of the overlay map. The results obtained are found to be unsatisfactory and in the case of language tasks the outcomes are much lower than those obtained in the studies aforementioned. To investigate why these values were low, we conducted two additional tests, which we call SC_1 and SC_2. The former is a sensitivity test while the second intended to find the contribution of rest activations in the overlap of the two maps. As the results obtained in SC_1 were quite higher than in DSC we can say that the number of undetected activations is restricted. This conclusion is highly relevant in the context of brain portions resection, since the removal of eloquent areas must be minimized: sensitivity more important than specificity in this context, because a false negative means that a relevant activated area went undetected and may end up removed by resection. Therefore we may conclude that the poor results of the DSC come from an excessive number of activated regions in resting-state, which if confirmed by the high levels of SC_2. This result confirms the need to extract independent components more fragmented (i.e. increase the number of IC), in order to improve the specificity of the results.

Chapter 6

Conclusion

The present study was carried out in the context of the current interest in understanding the usefulness of resting state networks in the clinical environment. This study aimed to assess the feasibility of using the resting state networks as a complementary approach to the classical procedure that resorts to task-based mapping of brain regions whose resection should be avoided in brain tumor surgery. The selected approach was to measure the similarity between the activation maps at rest of a subject with the activation maps of each task to the same subject.

With this goal in mind, a pre-processing protocol was devised and tested in order to obtain images which provide an optimal extraction of activation networks. The resulting images were then processed. The approaches conducted for processing rest and task images were different and were adapted from those already reported in the literature. The resemblance of these maps was subsequently evaluated using several similarity coefficients.

The obtained results allowed to conclude that the selected methodology is remarkably sensitive to activated regions detection and its extension. However a reduced specificity is found which results from an inefficient detection of common activations at rest and task. Nonetheless, even though low specificity restricts the application of rs-fMRI as a exclusive method of mapping important regions of the brain, high sensitivity shows that resting state fMRI could become a complementary method to the task-based classic approach in the future.

In order for rs-fMRI to be widely used as a complement to task-based fMRI, further studies will be required to improve these results. Some pre-processing and processing procedures may be reevaluated, namely those that contradict what is described in the literature. A refinement of the procedure for rest network detection, including optimization for single-subject analysis as opposed to groups, is also contemplated in order to improve the specificity of the method. Another interesting approach would also be to reproduce this study to other clinical cases referred for surgical resection of portions of the brain, such as epilepsy, in order to understand how the different disorders may affect communication in the brain at rest and consequently assess how is that hypothetical change could lead to a greater resemblance to the regions activated by task.

It should be stressed that this thesis was carried out as part of an ongoing project that involves collaboration with clinical partners. Several refinements, including the ones mentioned above, are expected to be implemented in this context, and thereby to bring about an improved performance of the protocols that are currently in place in a clinical setting

Bibliography

[1] M. K. Sidhu, J. Stretton, G. P. Winston, A. W. McEvoy, M. Symms, P. J. Thompson, M. J. Koepp, and J. S. Duncan, "Memory network plasticity after temporal lobe resection : a longitudinal functional imaging study", *Brain*, vol. 139, no. Pt 2, pp. 1–16, 2016.

[2] F. Pittau, P. Mégevand, L. Sheybani, E. Abela, F. Grouiller, L. Spinelli, C. M. Michel, M. Seeck, and S. Vulliemoz, "Mapping epileptic activity : sources or networks for the clinicians ?", *Frontiers in Neurology*, vol. 5, no. 1, pp. 1–21, 2014.

[3] D. Zhang, J. M. Johnston, M. D. Fox, C Eric, R. L. Grubb, M. R. Chicoine, M. D. Smyth, A. Z. Snyder, M. E. Raichle, and J. S. Shimony, "Preoperative Sensorimotor Mapping in Brain Tumor Patients using Spontaneous Fluctuations in Neuronal Activity Imaged with fMRI: Initial Experience", *Neurosurgery*, vol. 65, no. 314, pp. 226–236, 2010.

[4] G. Spena, A. Nava, F. Cassini, A. Pepoli, M. Bruno, F. D'Agata, F. Cauda, K. Sacco, S. Duca, L. Barletta, and P. Versari, "Preoperative and intraoperative brain mapping for the resection of eloquent-area tumors. A prospective analysis of methodology, correlation, and usefulness based on clinical outcomes", *Acta Neurochirurgica*, vol. 152, no. 11, pp. 1835–1845, 2010.

[5] K. E. Weaver, W. A. Chaovalitwongse, E. J. Novotny, A Poliakov, T. G. Grabowski, and J. G. Ojemann, "Local functional connectivity as a pre-surgical tool for seizure focus identification in non-lesion, focal epilepsy", *Frontiers in Neurology*, vol. 4, no. 43, pp. 1–14, 2013.

[6] C. Rosazza, D. Aquino, L. D'Incerti, R. Cordella, A. Andronache, D. Zacà, M. G. Bruzzone, G. Tringali, and L. Minati, "Preoperative mapping of the sensorimotor cortex: Comparative assessment of task-based and resting-state fMRI", *PLoS ONE*, vol. 9, no. 6, pp. 1–19, 2014.

[7] M. P. van den Heuvel and H. E. Hulshoff Pol, "Exploring the brain network: A review on resting-state fMRI functional connectivity", *European Neuropsychopharmacology*, vol. 20, no. 8, pp. 519–534, 2010.

[8] M. D. Fox and M Greicius, "Clinical applications of resting state functional connectivity", *Frontiers in systems neuroscience*, vol. 4, no. June, pp. 1–137, 2010.

[9] M. F. Bear, B. W. Connors, and M. A. Paradiso, "The Structure of the Nervous System", in *Neuroscience - Exploring the brain*, E. Lupash, Ed., 3rd Edition, Baltimore: Lippincott Williams & Wilkins, 2006, ch. Chapter 7, pp. 168 –204.

[10] V. Stark-Vance and M. L. Dubay, "The basics", in *100 Questions & answers about brain tumors*, Sudbury, Massachusetts: Jones & Bartlett Learning, 2010, ch. 1st Chapte, pp. 1–4, ISBN: 1449630995.

[11] R. T. Merrell, "Brain Tumors", *Disease-a-Month*, vol. 58, no. 12, pp. 678–689, 2012.

[12] H. Marsh, "Brain tumours", *Surgery (Oxford)*, vol. 27, no. 3, pp. 135–138, 2009.

[13] *What You Need To Know About Brain Tumors*. 2009, pp. 1–51.

[14] D. Glass-Macenka, "Understanding brain tumors.", in *Frankly Speaking about cancer*, T. J. Hopkins, Ed., 2008, pp. 5–14.

[15] D. A. Hardesty and P. Nakaji, "The Current and Future Treatment of Brain Metastases", *Frontiers in Surgery*, vol. 3, no. May, pp. 1–7, 2016.

[16] J. M. González, "Management of Brain Tumors in Eloquent Areas", in *Diagnostic Techniques and Surgical Management Of Brain Tumors*, A. L. Abujamra, Ed., 3rd Edition, Rijeka, Croatia: InTech, 2011, ch. 25, pp. 168 –204.

[17] M. G. Allen, A. Z. Snyder, C. D. Hacker, T. J. Mitchell, E. C. Leuthardt, and J. S. Shimony, "Task-Based Presurgical Functional MRI in Patients with Brain Tumors", in *Clinical Functional MRI: Presurgical Functional Neuroimaging*, A. B. B. Leuven, M. K. Göttingen, and K. S. Heidelberg, Eds., Berlin: Springer, 2007, ch. 4, pp. 143–158.

[18] M. Ragnehed, "Clinical application of functional MRI.", in *Functional magnetic resonance imaging for clinical diagnosis- exploring and improving the examination chain*, 1121, vol. 34, Linköping: Elsevier, 2009, ch. 4, pp. 267–277.

[19] S. Borchers, M. Himmelbach, N. Logothetis, and H.-O. Karnath, "Direct electrical stimulation of human cortex - the gold standard for mapping brain functions?", *Nature reviews. Neuroscience*, vol. 13, no. 1, pp. 63–70, 2012.

[20] M. J. Hamberger and J. Cole, "Language organization and reorganization in epilepsy", *Neuropsychology Review*, vol. 21, no. 3, pp. 240–251, 2011.

[21] M. F. Hartshorne, "Positron emission tomography", in *Functional Brain Imaging*, vol. 187, St. Louis: Elsevier Health Sciences, 1995, ch. 5, pp. 187–212.

[22] J. Brito, "Dynamic Functional Connectivity of BOLD fMRI signal during both rest and task execution states Dynamic Functional Connectivity of BOLD fMRI signal during both rest and task execution states", Master's thesis, 2014, pp. 1–2.

[23] E. W. Pang and O. C. Snead III, "From Structure to Circuits: The Contribution of MEG Connectivity Studies to Functional Neurosurgery", *Frontiers in Neuroanatomy*, vol. 10, no. June, pp. 1–14, 2016.

[24] C. G. Roth, "Introduction to Body MRI", in *Fundamentals of Body MRI*, 3, vol. 264, Elsevier Health Sciences, 2012, ch. 1, pp. 1–34.

[25] K. Uludag, D. J. Dubowitz, and R. B. Buxton, "Clinical magnetic resonance imaging", in *Clinical MRI. Elsevier, San Diego*, R. R. Edelman, J. Hesselink, and M. Zlatkin, Eds., 3rd Editio, Philadelphia: Saunders Elsevier, 2006, ch. 9, pp. 249–287.

[26] M. Ragnehed, "Funtcitonal MRI", in *Functional Magnetic Resonance imaging for clinical diagnosis - exploring and improving the examination chain*, 1121, Sweden: LiU-tryck, 2009, ch. 3.

[27] J. C. Gore, "Principles and practice of functional MRI of the human brain", *Journal of Clinical Investigation*, vol. 112, no. 1, pp. 4–9, 2003.

[28] H Mao and G. S. Berns, "MRI in the study of brain functions : clinical perspectives", *MedicaMundi*, vol. 46, no. 1, pp. 28–38, 2002.

[29] S. Yorkwilliams and K. L. Poston, "What light have resting state fMRI studies shed on cognition and mood in Parkinson ' s disease ?", *Journal of Clinical Movement Disorders*, vol. 1, no. 1, pp. 1–12, 2014.

[30] S. Li, A. Eloyan, S. Joel, S. Mostofsky, J. Pekar, S. S. Bassett, and B. Caffo, "Analysis of Group ICA-Based Connectivity Measures from fMRI: Application to Alzheimer's Disease", *PLoS ONE*, vol. 7, no. 11, pp. 1–10, 2012.

[31] A. Z. Snyder and M. E. Raichle, "A Brief History of the Resting State: the Washington University Perspective", *NeuroImage*, vol. 62, no. 2, pp. 902–910, 2012.

[32] S. S. Kety and C. F. Schmidt, "The nitrous oxide method for the quantative determination of cerebral blood flow in man: theory, procedure and normal values", *The Journal of clinical investigation*, vol. 27, no. 4, pp. 476–483, 1948.

[33] P. L. Purdon and R. M. Weisskoff, "Effect of temporal autocorrelation due to physiological noise and stimulus paradigm on voxel-level false-positive rates in fMRI", *Human Brain Mapping*, vol. 6, no. 4, pp. 239–249, 1998.

[34] K. J. Friston, S Williams, R Howard, R. S. Frackowiak, and R Turner, "Movement-related effects in fMRI time-series", *Magnetic resonance in medicine*, vol. 35, no. 3, pp. 346–355, 1996.

[35] B. B. Biswal, "Resting state fMRI: A personal history", in *NeuroImage*, 2, vol. 62, Elsevier Inc., 2012, pp. 938–944.

[36] D. Cordes, V. M. Haughton, K. Arfanakis, G. J. Wendt, P. A. Turski, C. H. Moritz, M. A. Quigley, and M. E. Meyerand, "Mapping functionally related regionsof brain with functional connectivity MR imaging", *American Society of Neuroradiology*, vol. 21, no. 9, pp. 1636–1644, 2000.

[37] R. L. Buckner, J. R. Andrews-Hanna, and D. L. Schacter, "The Brain's Default Network", *Annals of the New York Academy of Sciences*, vol. 1124, no. 1, pp. 1–38, 2008.

[38] L. Heine, A. Soddu, F. Gómez, A. Vanhaudenhuyse, L. Tshibanda, M. Thonnard, V. Charland-Verville, M. Kirsch, S. Laureys, and A. Demertzi, "Resting state networks and consciousness Alterations of multiple resting state network connectivity in physiological, pharmacological, and pathological consciousness states", *Frontiers in Psychology*, vol. 3, no. August, pp. 1–12, 2012.

[39] J. C. Tamraz and Y. G. Comair, "Central Region and Motor Cortex", in *Atlas of Regional Anatomy of the Brain Using MRI*, 2005, ch. 4, pp. 51–116.

[40] M. H. Lee, C. D. Smyser, and J. S. Shimony, "Resting state fMRI: A review of methods and clinical applications", *American Journal of Neuroradiology*, vol. 34, no. 10, pp. 1866–1872, 2013.

[41] *Radiology Key*. [Online]. Available: `http://radiologykey.com/magnetic-resonance-imaging-2/` (visited on 08/01/2016).

[42] H. I. Sair, N. Yahyavi-Firouz-Abadi, V. D. Calhoun, R. D. Airan, S. Agarwal, J. Intrapiromkul, A. S. Choe, S. K. Gujar, B. Caffo, M. A. Lindquist, and J. J. Pillai, "Presurgical brain mapping of the language network in patients with brain tumors using resting-state fMRI: Comparison with task fMRI", *Human Brain Mapping*, vol. 37, no. 3, pp. 913–923, 2016.

[43] P. Branco, D. Seixas, S. Deprez, S. Kovacs, R. Peeters, S. L. Castro, and S. Sunaert, "Resting-State Functional Magnetic Resonance Imaging for Language Preoperative Planning", *Frontiers in human neuroscience*, vol. 10, no. February, pp. 1–14, 2016.

[44] Y. Tie, L. Rigolo, I. H. Norton, R. Y. Huang, W. Wu, D. Orringer, S. Mukundan, and A. J. Golby, "Defining language networks from resting-state fMRI for surgical planning- A feasibility study", *Human Brain Mapping*, vol. 35, no. 3, pp. 1018–1030, 2014.

[45] C. M. Bennett, G. L. Wolford, and M. B. Miller, "The principled control of false positives in neuroimaging", *Social Cognitive and Affective Neuroscience*, vol. 4, no. 4, pp. 417–422, 2009.

[46] J. R. Andrews-Hanna, A. Z. Snyder, J. L. Vincent, C. Lustig, D. Head, M. E. Raichle, and R. L. Buckner, "Disruption of large-scale brain systems in advanced aging", *Neuron*, vol. 56, no. 5, pp. 924–935, 2007.

[47] M. D. Iglesia-vaya, J. Molina-mateo, M. J. Escarti-fabra, A. S. Kanaan, and L. Martí-bonmatí, "Brain Connections – Resting State fMRI Functional Connectivity", in *Novel Frontiers of Advanced Neuroimaging*, K. N. Fountas, Ed., 2013, ch. 3, pp. 51–66.

[48] Y. Golland, P. Golland, S. Bentin, and R. Malach, "Data-driven clustering reveals a fundamental subdivision of the human cortex into two global systems", *Neuropsychologia*, vol. 46, no. 2, pp. 540–553, 2008.

[49] M. H. Lee, C. D. Hacker, A. Z. Snyder, M. Corbetta, D. Zhang, E. C. Leuthardt, and J. S. Shimony, "Clustering of resting state networks", *PLoS ONE*, vol. 7, no. 7, pp. 1–12, 2012.

[50] S. M. H. N. Suma, "Principal Component Analysis for Analysis and Classification of fMRI Activation Maps", *Journal of Computer Science and network security*, vol. 7, no. 11, pp. 235–242, 2007.

[51] K. Friston, C. Frith, P. Liddle, and R. Frackowiak, "Functional Connectivity : The Principal-Component Analysis of Large (PET) Data Sets", *Journal of Cerebral Blood Flow & Metabolism*, vol. 13, no. 1, pp. 5–14, 1993.

[52] J. Damoiseaux, S. Rombouts, F Barkhof, P Scheltens, C. Stam, S. M. Smith, and C. Beckmann, "Consistent resting-state networks across healthy subjects", *Proceedings of the national academy of sciences*, vol. 103, no. 37, pp. 13 848–13 853, 2006.

[53] V. Kiviniemi, J.-H. Kantola, J. Jauhiainen, A. Hyvärinen, and O. Tervonen, "Independent component analysis of nondeterministic fMRI signal sources", vol. 19, no. 2, pp. 253–260, 2003.

[54] C. F. Beckmann, M. Deluca, J. T. Devlin, S. M. Smith, J. R. Hospital, and O. Ox, "Investigations into resting-state connectivity using independent component analysis", no. May, pp. 1001–1013, 2005.

[55] C. G. Yan, B Cheung, C Kelly, S Colcombe, R. C. Craddock, A Di Martino, Q Li, X. N. Zuo, F. X. Castellanos, and M. P. Milham, "A comprehensive assessment of regional variation in the impact of micromovement head motion on functional connectomics", *Neuroimage*, vol. 76, pp. 183–201, 2013.

[56] J. D. Power, K. A. Barnes, A. Z. Snyder, B. L. Schlaggar, and S. E. Petersen, "Spurious but systematic correlations in functional connectivity MRI networks arise from subject motion", *NeuroImage*, vol. 59, no. 3, pp. 2142–2154, 2012.

[57] T. D. Satterthwaite, D. H. Wolf, J. Loughead, K. Ruparel, M. A. Elliott, H. Hakonarson, R. C. Gur, and R. E. Gur, "Impact of in-scanner head motion on multiple measures of functional connectivity: Relevance for studies of neurodevelopment in youth", *NeuroImage*, vol. 60, no. 1, pp. 623–632, 2012.

[58] M. N. Hallquist, K. Hwang, and B. Luna, "The nuisance of nuisance regression: Spectral misspecification in a common approach to resting-state fmri preprocessing reintroduces noise and obscures functional connectivity", *Neuroimage*, vol. 82, pp. 208–225, 2013.